INFORMATION TO USERS

This manuscript has been reproduced from the microfilm master. UMI films the text directly from the original or copy submitted. Thus, some thesis and dissertation copies are in typewriter face, while others may be from any type of computer printer.

The quality of this reproduction is dependent upon the quality of the copy submitted. Broken or indistinct print, colored or poor quality illustrations and photographs, print bleedthrough, substandard margins, and improper alignment can adversely affect reproduction.

In the unlikely event that the author did not send UMI a complete manuscript and there are missing pages, these will be noted. Also, if unauthorized copyright material had to be removed, a note will indicate the deletion.

Oversize materials (e.g., maps, drawings, charts) are reproduced by sectioning the original, beginning at the upper left-hand corner and continuing from left to right in equal sections with small overlaps.

ProQuest Information and Learning
300 North Zeeb Road, Ann Arbor, MI 48106-1346 USA
800-521-0600

Université d'Ottawa · University of Ottawa

BIFURCATION ANALYSIS OF A CLASS OF DELAY-DIFFERENTIAL EQUATIONS WITH REFLECTIONAL SYMMETRY: APPLICATIONS TO ENSO

By
Brian F. Redmond, B.Sc.
August 2002

A Thesis
submitted to the School of Graduate Studies and Research
in partial fulfillment of the requirements
for the degree of
Master of Science in Mathematics[1]

[1]The M.Sc. Program is a joint program with Carleton University, administered by the Ottawa-Carleton Institute of Mathematics and Statistics

Abstract

We consider a general class of first-order nonlinear delay-differential equations (DDEs) with reflectional symmetry, and study completely the bifurcations of the trivial equilibrium under some generic conditions on the Taylor coefficients of the DDE. Our analysis reveals a Hopf bifurcation curve terminating on a pitchfork bifurcation line at a codimension two Takens-Bogdanov point in parameter space. We compute the normal form coefficients of the reduced vector field on the centre manifold in terms of the Taylor coefficients of the original DDE, and in contrast to many previous bifurcation analyses of DDEs, we also compute the unfolding parameters in terms of these coefficients. For application purposes, this is important since one can now identify the possible asymptotic dynamics of the DDE near the bifurcation points by computing quantities which depend explicitly on the Taylor coefficients of the original DDE. We illustrate these results using simple model systems relevant to the areas of neural networks and atmospheric physics, and show that the results agree with numerical simulations. Finally, note that most of the results of this thesis have already been refereed and published elsewhere (see [26]).

Acknowledgements

I would like to thank Victor G. LeBlanc and André Longtin for being excellent thesis supervisors and teachers, and for providing me with financial support. I would also like to thank the Department of Mathematics and Statistics at the University of Ottawa for financial support.

Dedication

I dedicate this work to my family.

Contents

Chapter 1

Introduction

In this thesis we consider the following class of scalar delay-differential equations

$$\frac{d}{dt}x(t) = f(x(t), x(t-\delta)), \tag{1}$$

where $\delta > 0$ is the delay, and f is an arbitrary smooth function which has reflectional symmetry in the following sense: $f(-a,-b) = -f(a,b)$ for all real a and b. The reflectional symmetry of f in (1) implies that $f(0,0) = 0$, i.e. the origin is an equilibrium solution. In this thesis, we will be interested in the bifurcations of this trivial equilibrium. Specifically we focus on the Taylor expansion of equation (1) around $(0,0)$, which yields, after a rescaling of time:

$$\begin{aligned}\frac{d}{dt}x(t) &= x(t) + \alpha x(t-\tau) + \gamma_1 x(t)^3 + \gamma_2\, x(t)^2\, x(t-\tau) \\ &\quad + \gamma_3\, x(t)\, x(t-\tau)^2 + \gamma_4\, x(t-\tau)^3 + O(|x|^5),\end{aligned} \tag{2}$$

where $\tau = D_1 f(0,0)\delta$, $\alpha = D_2 f(0,0)/D_1 f(0,0)$, $\gamma_1 = D_{111} f(0,0)/6D_1 f(0,0)$, $\gamma_2 = D_{112} f(0,0)/2D_1 f(0,0)$, $\gamma_3 = D_{122} f(0,0)/2D_1 f(0,0)$, and $\gamma_4 = D_{222} f(0,0)/6D_1 f(0,0)$. In our notation, $D_i f(0,0)$ denotes the first-order partial derivative of the function f with respect to its i^{th} argument ($i = 1, 2$), evaluated at $(0,0)$, with similar notation used for higher order partial derivatives. Here we have assumed that the Taylor coefficient $D_1 f(0,0)$ is positive in order to achieve a coefficient of 1 for the $x(t)$ term in (2). We will see that in this case codimension one bifurcation curves can intersect,

leading to a codimension two bifurcation point. The case where $D_1 f(0,0) < 0$ can be studied without any added difficulty. However, it is a somewhat simpler case in the sense that the codimension one bifurcation curves do not intersect [3]; it has in fact been previously treated elsewhere in the literature (see e.g. [2, 15]).

Equation (2) encompasses a wide variety of possible physical situations. For example, the case

$$\frac{d}{dt}x(t) = x(t) - x(t)^3 + \alpha\, x(t-\tau) \tag{3}$$

corresponds to the equation of motion of a particle in an overdamped bistable symmetric potential known as the "standard quartic" potential, with an additional linear force due to its motion in the past. The motion in the absence of delayed feedback has two coexisting fixed points, separated by the unstable origin. Whether this delayed force is restoring or not (with respect to the origin) may depend on its magnitude and sign, which in turn will depend on the full dynamics of the system. In particular, we will see that our bifurcation analysis of such a system reveals parameter regions where the origin is stabilized by this delayed force.

The fact that the origin is unstable even without delayed feedback is a distinguishing feature of the DDE class equation (2). This is in contrast with work on e.g. neural circuits and networks with one [2, 5, 23] or more [6, 8, 9, 16, 31, 32, 33] delays. Our particular interest in this class of DDE's stems from their relevance to coupled bistable detector arrays [14, 21]. Such arrays can use noise and coupling to synchronize transitions between states to the fluctuations of small input signals, thereby amplifying these signals. We are currently extending the coupling of such elements to include delayed feedback. This connectivity is suggested in particular by neural circuitry involved in signal detection and processing (see e.g. [4] and references therein). In this context, it is known that bistable systems are also a good approximation to the dynamics of certain neurons [7, 22]. In particular, they have recently been shown to be powerful building blocks for neural networks performing associative memory tasks [11]. Further, there has also been a recent study of combined bistability and delay and noise in the context of a simple neuron model [25].

Thus, inspired by research on bistable systems and on neural dynamics and information processing, we have been developing versions of such neural networks and

detector arrays that include delayed feedback. It has become crucial, in this context, to understand the basic dynamics of bistability with feedback. We also anticipate that the dynamics studied here will be of relevance to studies of chemical reactions with global delayed feedback (see [20] and references therein).

Specific instances of equation (2) have also found applications in atmospheric physics, namely as early heuristic models of the El Niño/Southern Oscillation (ENSO) phenomenon [1, 28]; this "delayed oscillator" approach to ENSO is summarized in Chapter 8 as a preamble to the examples chosen to illustrate our analytical results. Such models had only been analyzed using linear stability analysis as well as numerical analysis; their full bifurcation analysis had not been done, and in particular, the presence of a codimension two bifurcation point had escaped earlier numerical analyses. Although current models of ENSO are more sophisticated, our analysis of these earlier models improves our understanding of the dynamical complexity that the delayed oscillator picture may hold in this and other contexts.

The thesis is organized as follows. In the next Chapter, we will study the linearized stability of the trivial equilibrium of (2), and show that in the (α, τ)-parameter space, there are two codimension one bifurcation curves: a Hopf bifurcation curve and a pitchfork curve. The Hopf curve terminates at the pitchfork curve in a point where the characteristic equation has a double zero root. This corresponds to a codimension two Takens-Bogdanov bifurcation of the trivial equilibrium. We next review the literature on the double zero eigenvalue in Chapter 3. This will include a normal form analysis and a bifurcation analysis. In Chapter 4, we briefly review the theory of centre manifold reduction for parameter dependent DDEs, and then in the next two Chapters we perform centre manifold reductions for both the Hopf and the pitchfork bifurcations in (2). In particular, we compute both the first Liapunov coefficient of the Hopf bifurcation, and the coefficient of the cubic term in the pitchfork normal form in terms of the coefficients α, τ and $\gamma_i, 1 \leq i \leq 4$, of (2). In Chapter 7, we study the Takens-Bogdanov bifurcation for (2). Because of the reflectional symmetry of f in (1), the centre manifold equations will also have reflectional symmetry. It is well-known that generically, there are two distinct topological types (normal forms) for this bifurcation. As a by-product of our analysis, we will give conditions on

the coefficients $\gamma_i, 1 \leq i \leq 4$, of (2) which determine which type of Takens-Bogdanov bifurcation will occur in (1). Thus, provided these generic conditions are satisfied, our analysis completely describes the local bifurcations of the trivial equilibrium solution in (1), *regardless of the fifth and higher order terms in (2).* Finally, in Chapter 8 we will illustrate our results with some numerical integrations of certain models which fall into the class of equations described by (1). A conclusion follows in Chapter 9.

Chapter 2

Linear stability analysis

In this Chapter we locate the region of stability of the equilibrium solution $x(t) = 0$ of equation (2). Linearizing (2) near this equilibrium solution we obtain

$$\frac{d}{dt}x(t) = x(t) + \alpha x(t-\tau). \tag{4}$$

Substitution of the ansatz $x(t) = e^{\lambda t}$ into (4), where λ is a complex parameter, gives the characteristic equation

$$\lambda = 1 + \alpha e^{-\lambda\tau}. \tag{5}$$

We have the following theorem (Theorem A.5 of [19]):

Theorem 1 (Hale and Lunel [19]) *All roots of the equation* $(z+a)e^z + b = 0$, *where* a *and* b *are real, have negative real parts if and only if*

$$\begin{aligned} &a > -1 \\ &a + b > 0 \\ &b < \zeta \sin\zeta - a\cos\zeta, \end{aligned} \tag{6}$$

where ζ *is the root of* $\zeta = -a\tan\zeta$, $0 < \zeta < \pi$, *if* $a \neq 0$ *and* $\zeta = \pi/2$ *if* $a = 0$.

Using Theorem 1 we find that all roots of (5) have negative real parts if and only if

$$\begin{aligned} &\tau < 1 \\ &\alpha < -1 \\ &\alpha\tau > -\zeta\sin\zeta - \tau\cos\zeta, \end{aligned} \tag{7}$$

where ζ is the root of $\zeta = \tau \tan\zeta$, $0 < \zeta < \pi$, and $\zeta = \pi/2$ if $\tau = 0$. Since τ must be positive (for the physically interesting case), the region defined by (7) is illustrated as the hashed region in Figure 1.

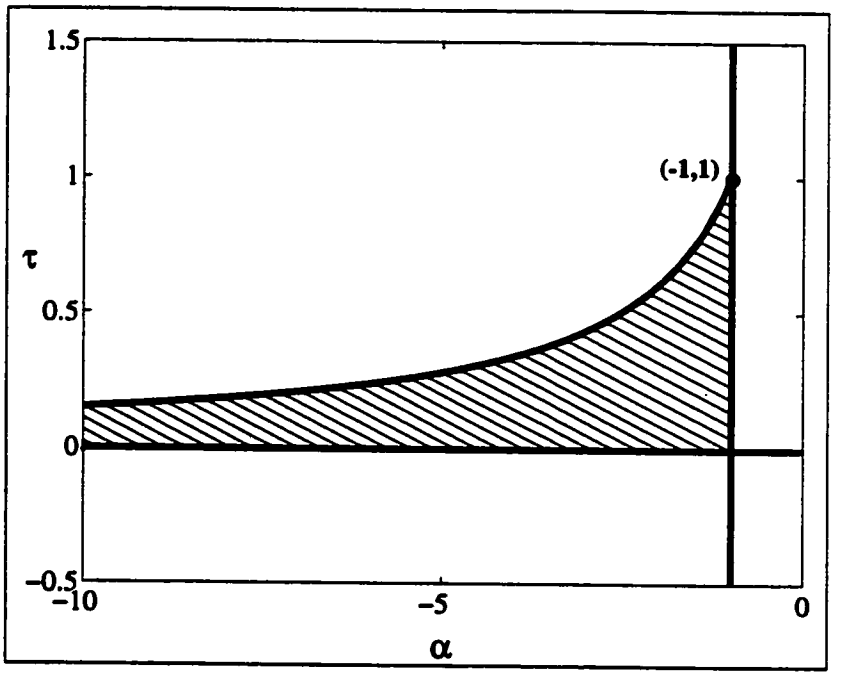

Figure 1: Stability diagram for the equilibrium solution $x(t) = 0$ of (2). Hashed area corresponds to the stability region.

On the top and right-hand boundaries of the hashed region in Figure 1, equation (5) has a finite number of solutions with zero real part, and all other solutions have negative real part. Therefore bifurcations occur for parameter values on these two curves. The top boundary curve is characterized by setting $\lambda = i\omega$ in (5). After separating real and imaginary parts in (5), we obtain

$$\begin{aligned} 1 &= -\alpha \cos\omega\tau \\ \omega &= -\alpha \sin\omega\tau. \end{aligned} \tag{8}$$

Squaring both equations and adding, we get

$$\omega = \pm\sqrt{\alpha^2 - 1}. \tag{9}$$

The right-hand boundary curve is characterized by setting $\lambda = 0$ in (5). This substitution gives

$$\alpha = -1. \tag{10}$$

We see that the right boundary line $\alpha = -1$ in Figure 1 is a line where the characteristic equation has a single zero root. Because of the reflectional symmetry of (2), this line corresponds to a pitchfork bifurcation curve. The top boundary curve in Figure 1 is a curve where the characteristic equation has purely imaginary complex conjugate roots (i.e. it is a Hopf bifurcation curve). At the point $(\alpha, \tau) = (-1, 1)$ where these two curves meet, (5) has a double zero root, i.e. (4) has two linearly independent solutions $x(t) = 1$ and $x(t) = t$. This point thus corresponds to a Takens-Bogdanov bifurcation.

Chapter 3

The double zero eigenvalue

3.1 Normal form analysis

Consider the equation $dx/dt = g(x)$ on $\mathbb{R}^2$, with g smooth and with reflectional symmetry, i.e. $g(-x) = -g(x)$ for all real $x \in \mathbb{R}^2$. Note that the reflectional symmetry of g implies that $g(0) = 0$. Taylor's theorem then allows us to write

$$\frac{d}{dt}x(t) = J\,x(t) + F_3(x(t)) + O(|x(t)|^5), \tag{11}$$

where $x = [z_1, z_2]^T \in \mathbb{R}^2$, J is a 2×2 matrix in Jordan canonical form, and F_3 consists entirely of third order terms. Note that the reflectional symmetry of g forces the quadratic and quartic terms to be zero. For the double zero eigenvalue case, we shall assume that J has the form

$$J = \begin{pmatrix} 0 & 1 \\ 0 & 0 \end{pmatrix}.$$

To begin with, we will reduce equation (11) to normal form (up to third order). For more details on normal form transformations, see e.g. [17]. We define $H_3^2 \equiv$ linear space of 2-vector valued homogeneous polynomials on 2-variables of degree 3. That is, let H_3^2 be the span of the following set of vectors

$$\left\{ \begin{pmatrix} z_1^3 \\ 0 \end{pmatrix}, \begin{pmatrix} z_1^2 z_2 \\ 0 \end{pmatrix}, \begin{pmatrix} z_1 z_2^2 \\ 0 \end{pmatrix}, \begin{pmatrix} z_2^3 \\ 0 \end{pmatrix}, \begin{pmatrix} 0 \\ z_1^3 \end{pmatrix}, \begin{pmatrix} 0 \\ z_1^2 z_2 \end{pmatrix}, \begin{pmatrix} 0 \\ z_1 z_2^2 \end{pmatrix}, \begin{pmatrix} 0 \\ z_2^3 \end{pmatrix} \right\}.$$

We now introduce the homological operator L_J on the space H_3^2 defined by

$$L_J[h_3(x)] \equiv Dh_3(x)Jx - Jh_3(x), \tag{12}$$

where $h_3(x) \in H_3^2$. It can easily be checked that L_J is linear. We now wish to solve the following equation for $h_3(x)$

$$L_J[h_3(x)] \equiv Dh_3(x)Jx - Jh_3(x) = F_3(x). \tag{13}$$

If F_3 is such that (13) can be solved for h_3, then the near-identity change of coordinates $x \to x + h_3(x)$ transforms (11) to

$$\frac{d}{dt}x(t) = J\,x(t) + O(|x(t)|^5). \tag{14}$$

However, in general it is not possible to solve (13) because L_J may not be invertible. We may, however, be able to eliminate many of the cubic terms. Discovering which terms can be eliminated is the goal of the next set of calculations. A general element $h_3(x) \in H_3^2$ has the form

$$\begin{pmatrix} a_1\,z_1^3 + a_2\,z_1^2z_2 + a_3\,z_1z_2^2 + a_4\,z_2^3 \\ a_5\,z_1^3 + a_6\,z_1^2z_2 + a_7\,z_1z_2^2 + a_8\,z_2^3 \end{pmatrix},$$

where $a_1, \ldots, a_8 \in \mathbb{R}$. It is easy to compute

$$L_J[h_3(x)] = \begin{pmatrix} -a_5\,z_1^3 + (3a_1 - a_6)\,z_1^2z_2 + (2a_2 - a_7)\,z_1z_2^2 + (a_3 - a_8)\,z_2^3 \\ 3a_5\,z_1^2z_2 + 2a_6\,z_1z_2^2 + a_7\,z_2^3 \end{pmatrix},$$

Thus,

$$L_J(H_3^2) = \text{span}\left\{ \begin{pmatrix} -z_1^3 \\ 3z_1^2z_2 \end{pmatrix}, \begin{pmatrix} z_1^2z_2 \\ 0 \end{pmatrix}, \begin{pmatrix} z_1z_2^2 \\ 0 \end{pmatrix}, \begin{pmatrix} z_2^3 \\ 0 \end{pmatrix}, \begin{pmatrix} 0 \\ z_1z_2^2 \end{pmatrix}, \begin{pmatrix} 0 \\ z_2^3 \end{pmatrix} \right\}.$$

So we see that

$$H_3^2 = L_J(H_3^2) \oplus G_3,$$

where

$$G_3 = \text{span}\left\{ \begin{pmatrix} 0 \\ z_1^3 \end{pmatrix}, \begin{pmatrix} 0 \\ z_1^2z_2 \end{pmatrix} \right\},$$

is the complimentary space to $L_J(H_3^2)$. Thus, although we cannot solve (13) completely, we can eliminate the terms of F_3 which lie in $L_J(H_3^2)$. So equation (11) can be reduced, by a nonlinear transformation of coordinates $x \to x + h_3(x)$, to a system of the form

$$\begin{aligned} \frac{d}{dt} z_1 &= z_2 + O(|x|^5) \\ \frac{d}{dt} z_2 &= a\, z_1^3 + b\, z_1^2 z_2 + O(|x|^5) \end{aligned} \tag{15}$$

where the constants a and b are determined by the coefficients in $F_3(x)$.

3.2 Bifurcation analysis

It is well-known [29] that the normal forms for the Takens-Bogdanov singularity with reflectional symmetry are determined to cubic order and are given by

$$\begin{aligned} \frac{d}{dt} x &= y, \\ \frac{d}{dt} y &= a\, x^3 + b\, x^2 y, \end{aligned} \tag{16}$$

when a and b are both non-zero. That is, the local dynamics near the origin for the full system (15) are topologically equivalent to the local dynamics near the origin for the truncated system (16). The following two-parameter family then provides a versal unfolding for (16) [17, §7.3]

$$\begin{aligned} \frac{d}{dt} x &= y, \\ \frac{d}{dt} y &= \beta_1\, x + \beta_2\, y + a\, x^3 + b\, x^2 y. \end{aligned} \tag{17}$$

Note that up to reflections and a reversal of time, there are precisely two topological normal forms in (17). These can be chosen to be the cases with (1) $a < 0$, $b < 0$, and (2) $a > 0$, $b < 0$. However, in our case time reversals are not possible since we are dealing with a DDE. Thus, we must also consider the two cases where $b > 0$. However, it is easy to see that these are obtained from the two standard cases by merely reversing the direction of the flow, reflecting the phase space across the y

axis, and reflecting the parameter space across the β_1 axis. We now consider each topological case individually.

Case 1: $a > 0$

In this case all possible dynamics near the Takens-Bogdanov point are summarized in Figure 2a for the case $b < 0$ (reverse the direction of the arrows, reflect the phase space across the y axis and reflect the parameter space across the β_1 axis for the case $b > 0$). The line $\beta_2 = 0$ ($\beta_1 < 0$) is a Hopf bifurcation line, and the line $\beta_1 = 0$ is a

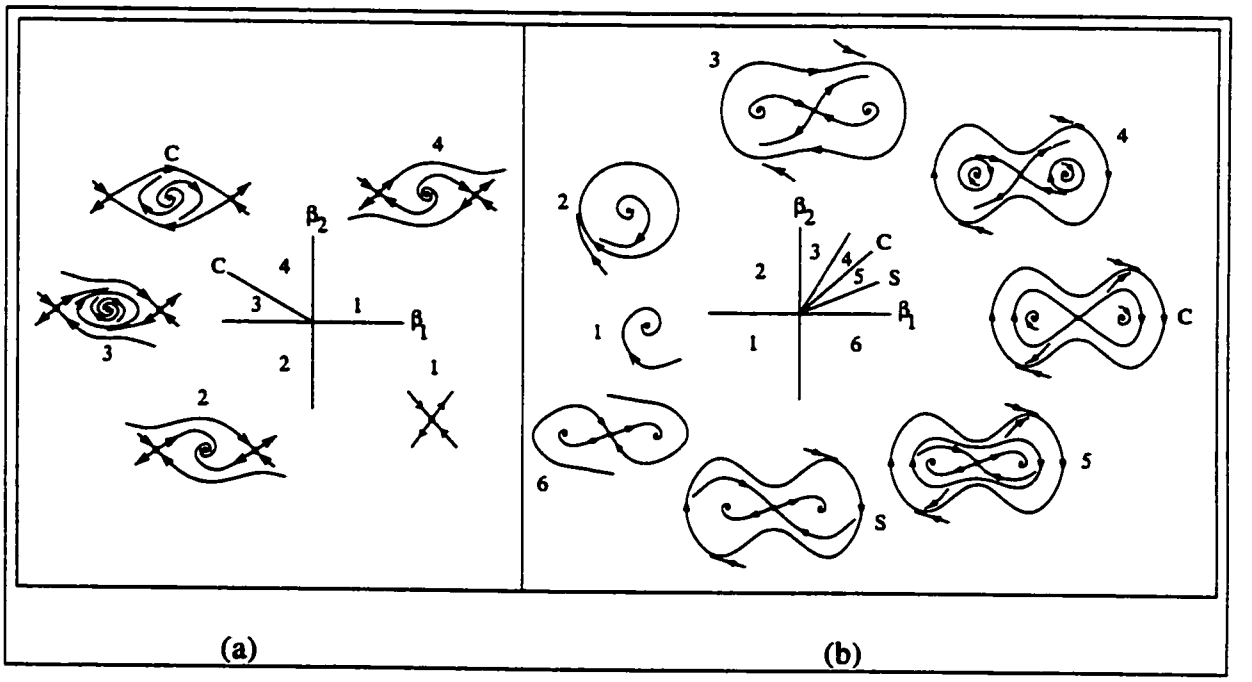

Figure 2: Unfolding of both topological cases of the Takens-Bogdanov bifurcation with reflectional symmetry. All possible dynamics near the Takens-Bogdanov point (the origin in this figure) are summarized. In (a) we have $a > 0$, $b < 0$ and in (b) we have $a < 0$, $b < 0$ in equation (17).

pitchfork bifurcation line. It remains to determine what line C is in Figure 2a. We make the following change of variables to system (17) (assuming $\beta_1 < 0$)

$$x = \sqrt{-\frac{\beta_1}{a}}\,u, \quad y = \frac{-\beta_1}{\sqrt{a}}\,v, \quad t \to \sqrt{-\beta_1}\,t \tag{18}$$

and obtain

$$\begin{aligned} \frac{d}{dt}u &= v, \\ \frac{d}{dt}v &= -u + \frac{\beta_2}{\sqrt{-\beta_1}}v + \frac{b}{a}\sqrt{-\beta_1}\,u^2 v + u^3. \end{aligned} \tag{19}$$

Since we are only looking for a linear approximation to line C in Figure 2a, we will set $\beta_2 = c\,\beta_1$, where c is a constant to be determined. So when $\beta_1 = 0$ equations (19) become the following integrable system

$$\begin{aligned} \frac{d}{dt}u &= v, \\ \frac{d}{dt}v &= -u + u^3, \end{aligned} \tag{20}$$

with Hamiltonian

$$H(u,v) = \frac{v^2}{2} + \frac{u^2}{2} - \frac{u^4}{4}. \tag{21}$$

The level curves of H are given in Figure 3. We see a double heteroclinic connection between the equilibria $(-1,0)$ and $(1,0)$. We will compute the Melnikov function (see e.g. [17]) for the top heteroclinic orbit (denoted γ^+), which corresponds to $H(u,v) = 1/4$, and which connects the equilibria $(-1,0)$ and $(1,0)$; the computation for the bottom heteroclinic orbit (denoted γ^-) is identical. We proceed as follows. For notational purposes we first rewrite system (19) as follows

$$\begin{aligned} \frac{d}{dt}u &= f_1(u,v) + \epsilon\, g_1(u,v) \\ \frac{d}{dt}v &= f_2(u,v) + \epsilon\, g_2(u,v), \end{aligned} \tag{22}$$

where, $f_1(u,v) = v$, $g_1(u,v) = 0$, $f_2(u,v) = -u + u^3$, $g_2(u,v) = -c\,v + \frac{b}{a}u^2 v$, and $\epsilon = \sqrt{-\beta_1}$. Then the Melnikov function (see e.g. [17]) is

$$\begin{aligned} M(c) &= \int_{-\infty}^{\infty} (f_1(u,v)g_2(u,v) - f_2(u,v)g_1(u,v))\,dt \\ &= \int_{-\infty}^{\infty} v\left(-c\,v + \frac{b}{a}u^2 v\right)\,dt \end{aligned} \tag{23}$$

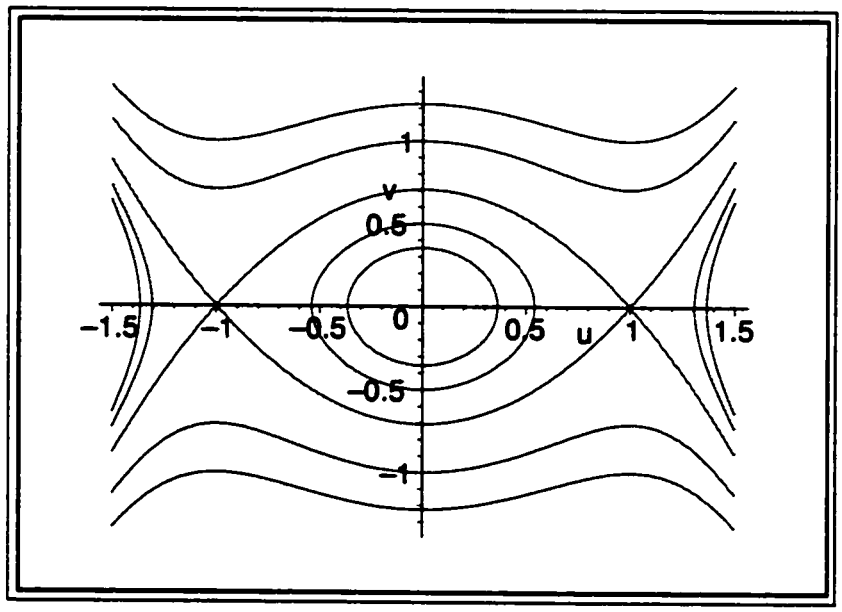

Figure 3: Level curves of H (21).

$$= -c\int_{\gamma^+} v\,du + \frac{b}{a}\int_{\gamma^+} u^2 v\,du, \tag{24}$$

$$= -\sqrt{2}\left(-c\int_0^1 (u^2-1)\,du + \frac{b}{a}\int_0^1 u^2(u^2-1)\,du\right), \tag{25}$$

$$= -\frac{2\sqrt{2}}{3}\left(c - \frac{1}{5}\frac{b}{a}\right) \tag{26}$$

where we have used $v = du/dt$ to convert the time integral into a contour integral over the top heteroclinic orbit γ^+ in Figure 3, and we have used $H(u,v) = 1/4$ to express v as a function of u. We see that $M(c)$ has a simple root for $c = \frac{1}{5}\frac{b}{a}$. And since $dM/d(c) \neq 0$, it can be shown (see [17]) that for parameters on the line

$$\beta_2 = \frac{1}{5}\frac{b}{a}\beta_1 + O(-\beta_1^{3/2}) \quad \text{and} \quad \beta_1 < 0, \tag{27}$$

system (17) (with $a > 0$, $b < 0$) has a double heteroclinic connection. Equation (27)

is line C of Figure 2a. This completes the bifurcation analysis for Case 1.

Case 2: $a < 0$

In this case all possible dynamics near the Takens-Bogdanov point are summarized in Figure 2b for the case $b < 0$ (reverse the direction of the arrows, reflect the phase space across the y axis and reflect the parameter space across the β_1 axis for the case $b > 0$). Let us investigate this case in a little more detail. The characteristic equation for system (17) for the equilibrium at the origin is

$$\lambda^2 - \beta_2\lambda - \beta_1 = 0, \tag{28}$$

with eigenvalues

$$\lambda = \frac{1}{2}\beta_2 \pm \frac{1}{2}\sqrt{\beta_2^2 + 4\beta_1}. \tag{29}$$

Thus, for $\beta_2 = 0$ and $\beta_1 < 0$ we have a pair of purely imaginary eigenvalues, and $d\mathrm{Re}\lambda/d\beta_2 = 1/2$. It follows from the Hopf Bifurcation Theorem that the line given by $\beta_2 = 0$ and $\beta_1 < 0$ is a Hopf bifurcation line. This is the line separating regions 1 and 2 in Figure 2b. We now show that the Hopf bifurcation is supercritical. We first use the linear transformation

$$P = \begin{pmatrix} 0 & 1/\sqrt{-\beta_1} \\ 1 & 0 \end{pmatrix},$$

to transform (17) (with $\beta_2 = 0$) into the following system

$$\begin{aligned} \frac{d}{dt}x &= -\sqrt{-\beta_1}\,y + a\,y^3/(-\beta_1)^{3/2} - b\,xy^2/\beta_1 \\ \frac{d}{dt}y &= \sqrt{-\beta_1}\,x \end{aligned} \tag{30}$$

Then, using formula (3.4.11) from [17], we get

$$a_{critical} = \frac{1}{16}\left(\frac{-2\,b}{\beta_1} + \frac{6\,a}{-\beta_1^{3/2}}\right). \tag{31}$$

So we see that in the case we are interested in ($\beta_1 < 0$, $a < 0$, $b < 0$) this coefficient is negative. Therefore the Hopf bifurcation is supercritical and Figure 2b is the correct phase diagram.

Next we consider the line $\beta_1 = 0$ in Figure 2b and show that this is a pitchfork bifurcation line. Indeed, when $\beta_1 = 0$ we see that (28) has a simple zero, and the linearized vector field near the origin has an associated right eigenvector $v = (1,0)^T$ and left eigenvector $w = (-\beta_2, 1)$. Also, if we let $f(\beta_1, x, y)$ denote the righthand side of (17), then we can check that

$$w\, f_{\beta_1}(0,0,0) = 0,$$

$$w\,[Df_{\beta_1}(0,0,0)\, v] = 1,$$

$$w\,[D^2 f(0,0,0)(v,v)] = 0,$$

$$w\,[D^3 f(0,0,0)(v,v,v)] = 6\,a.$$

It follows (see [17]) that the line $\beta_1 = 0$ is a pitchfork bifurcation line for the trivial equilibrium. Furthermore, since the ratio $w[D^3 f(0,0,0)(v,v,v)]/w[Df_{\beta_1}(0,0,0)\, v] = 6\,a/1 < 0$ (since $a < 0$ in this case), the two nontrivial fixed points appear for $\beta_1 > 0$, as is shown in Figure 2b. The criticality of this bifurcation is given by the sign of the product $-\beta_2\, a$. The bifurcation is supercritical if $\beta_2 < 0$ and subcritical if $\beta_2 > 0$.

Continuing our clockwise path around the origin in Figure 2b which began in region 1, we arrive at the line separating regions 3 and 4 in Figure 2b. We will show that this is a Hopf bifurcation line for the nontrivial fixed points. Indeed, we saw in the last paragraph that as we pass from region 2 into region 3 two nontrivial fixed points appear via a pitchfork bifurcation. These nontrivial fixed points are given by $(x, y) = (\pm\sqrt{-\beta_1/a}, 0)$. By symmetry we only need to consider one of the nontrivial fixed points. Centering system (17) around one of these fixed points and linearizing, we obtain the following characteristic equation

$$\lambda^2 + \left(\frac{b}{a}\beta_1 - \beta_2\right)\lambda + 2\,\beta_1 = 0, \tag{32}$$

with eigenvalues

$$\lambda = \frac{1}{2}\left(\beta_2 - \frac{b}{a}\beta_1\right) \pm \frac{1}{2}\sqrt{\left(\frac{b}{a}\beta_1 - \beta_2\right)^2 - 8\,\beta_1}. \tag{33}$$

Thus, to obtain a complex pair of pure imaginary eigenvalues, we must have

$$\beta_2 = \frac{b}{a}\beta_1 \quad \text{and} \quad \beta_1 > 0 \tag{34}$$

which is the line separating regions 3 and 4 in Figure 2b. It can be shown using the same technique as before that this bifurcation is indeed a Hopf and is subcritical. And this concludes the linear analysis of system (17). Lines C and S in Figure 2b will be derived using nonlinear analysis.

On line C we have a double homoclinic connection of the trivial equilibrium. To show this and to derive a linear approximation to line C, we proceed as follows. We make the following change of variables to system (17) (assuming $\beta_1 > 0$)

$$x = \sqrt{-\frac{\beta_1}{a}}\,u, \quad y = \frac{\beta_1}{\sqrt{-a}}\,v, \quad t \to \sqrt{\beta_1}\,t \tag{35}$$

and obtain

$$\begin{aligned} \frac{d}{dt}u &= v, \\ \frac{d}{dt}v &= u + \frac{\beta_2}{\sqrt{\beta_1}}v - \frac{b}{a}\sqrt{\beta_1}\,u^2 v - u^3. \end{aligned} \tag{36}$$

Again we write $\beta_2 = c\beta_1$, where c is a constant to be determined. So when $\beta_1 = 0$ equations (36) become the following integrable system

$$\begin{aligned} \frac{d}{dt}u &= v, \\ \frac{d}{dt}v &= u - u^3. \end{aligned} \tag{37}$$

with Hamiltonian

$$H(u,v) = \frac{v^2}{2} - \frac{u^2}{2} + \frac{u^4}{4}. \tag{38}$$

The level curves of H are given in figure 4. We see that a double homoclinic orbit occurs for $H(u,v) = 0$. We will compute the Melnikov function for the right homoclinic orbit (denoted γ^+) as follows; the computation for the left homoclinic orbit (denoted γ^-) is identical. For notational purposes we first rewrite system (36) as follows

$$\begin{aligned} \frac{d}{dt}u &= f_1(u,v) + \epsilon\, g_1(u,v) \\ \frac{d}{dt}v &= f_2(u,v) + \epsilon\, g_2(u,v), \end{aligned} \tag{39}$$

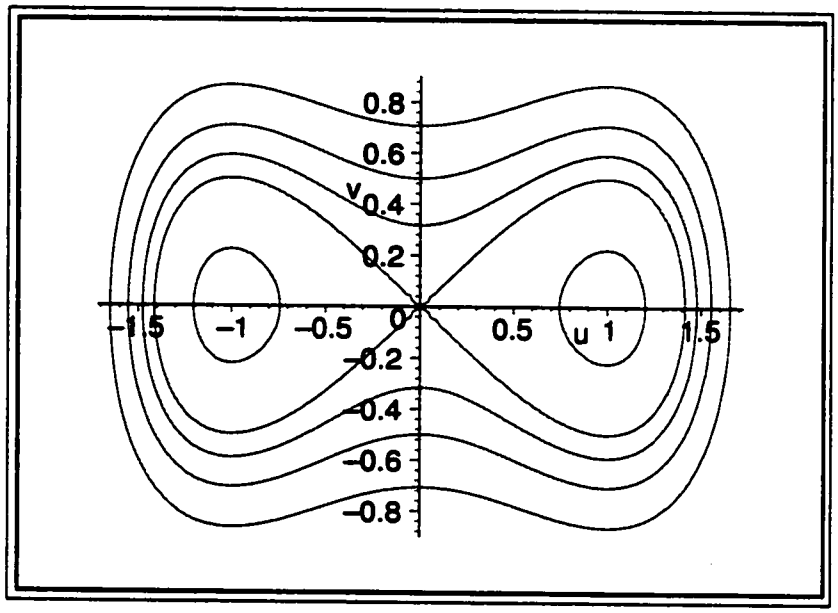

Figure 4: Level curves of H (38).

where, $f_1(u,v) = v$, $g_1(u,v) = 0$, $f_2(u,v) = u - u^3$, $g_2(u,v) = cv - \frac{b}{a}u^2 v$, and $\epsilon = \sqrt{\beta_1}$. Then

$$M(c) = \int_{-\infty}^{\infty} (f_1(u,v)g_2(u,v) - f_2(u,v)g_1(u,v))\, dt \tag{40}$$

$$= \int_{-\infty}^{\infty} v\left(cv - \frac{b}{a}u^2 v\right) dt$$

$$= c\int_{\gamma^+} v\, du - \frac{b}{a}\int_{\gamma^+} u^2 v\, du \tag{41}$$

$$= 2\left(c\int_0^{\sqrt{2}} u\sqrt{1-u^2/2}\, du - \frac{b}{a}\int_0^{\sqrt{2}} u^3\sqrt{1-u^2/2}\, du\right) \tag{42}$$

$$= \frac{4}{3}\left(c - \frac{4}{5}\frac{b}{a}\right), \tag{43}$$

where we have used $v = du/dt$ to convert the time integral into a contour integral over the right closed homoclinic orbit in Figure 4, and we have used $H(u,v) = 0$ to express v as a function of u. We see that $M(c) = 0$ has a simple zero for $c = \frac{4}{5}\frac{b}{a}$.

And since $dM/d(c) = 4/3 \neq 0$, it can be shown (see [17]) that for parameters on the line

$$\beta_2 = \frac{4}{5}\frac{b}{a}\beta_1 + O(\beta_1^{3/2}) \quad \text{and} \quad \beta_1 > 0. \tag{44}$$

system (17) (with $a < 0$, $b < 0$) has a double homoclinic connection. Equation (44) is line C of Figure 2b. To determine any information about the saddle node (of periodic orbits) bifurcation, we must also study the perturbations of the closed level curves lying within and outside of the double homoclinic orbit in Figure 4. This was done by Carr [10]. Let $\gamma = (u(t), v(t))$ denote one such level curve with hamiltonian value h and period T. Using Melnikov theory we get the following Melnikov function

$$\begin{aligned} M(\beta_1, \beta_2) &= \int_0^T (f_1(u,v)g_2(u,v) - f_2(u,v)g_1(u,v))\, dt \qquad (45) \\ &= \int_0^T v(t)\left(\frac{\beta_2}{\beta_1}v(t) - \frac{b}{a}u(t)^2 v(t)\right) dt \\ &= \frac{\beta_2}{\beta_1}\int_\gamma v\, du - \frac{b}{a}\int_\gamma u^2 v\, du, \qquad (46) \end{aligned}$$

where we have used $v = du/dt$ to convert the time integral into a contour integral on the closed orbit γ. Using the Hamiltonian (38), we can express v as a function of u and h for integration. For a given closed orbit to remain after perturbation, we must have $M = 0$, or

$$\frac{a}{b}\frac{\beta_2}{\beta_1} = \frac{\int_\gamma u^2 v\, du}{\int_\gamma v\, du} \stackrel{\text{def}}{=} R(h). \tag{47}$$

By numerical integration we plot $R(h)$ in Figure 5 (with limits of integration $u = 0$, $u = \sqrt{1+\sqrt{1+4h}}$). The function $R(h)$ has a unique minimum at energy value $h_s \approx 0.089$ giving an approximate value of 0.752 for R. Solving equation (47) for β_2 when $R = 0.752$ gives

$$\beta_2 \approx 0.752\frac{b}{a}\beta_1 \quad \text{and} \quad \beta_1 > 0, \tag{48}$$

which is the linear approximation to line S in Figure 2b, the saddle node bifurcation of periodic orbits. This completes the bifurcation analysis of system (17) in Case 2.

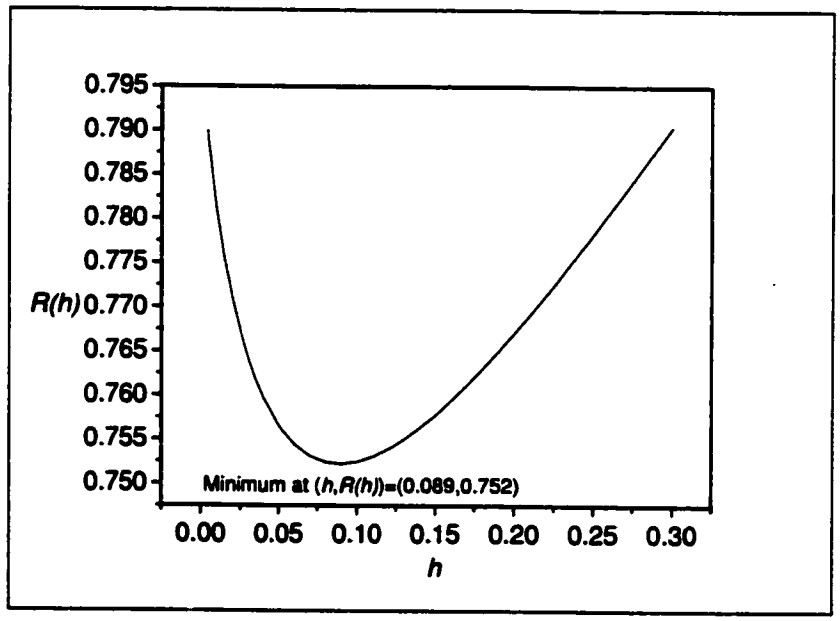

Figure 5: Zeros of the Melnikov function as a function of the energy value h. For $R(h) < 0.752$, no limit cycles survive the perturbation. When $R(h) = 0.752$, approximately, exactly one limit cycle survives the perturbation. This corresponds to the saddle node bifurcation of periodic orbits. For $R(h) > 0.752$, two limit cycles survive the perturbation; one stable and the other unstable.

Chapter 4

Centre manifold reduction with DDEs

In this Chapter, we briefly summarize the theory for centre manifold reductions of DDEs with parameters (see for example [12], [13], [18], and [19]). In the next two chapters we will apply these results to compute normal forms for both the Hopf and pitchfork bifurcations of the trivial equilibrium in (2). We will perform a similar analysis for the Takens-Bogdanov bifurcation in Chapter 7.

We first let $X \stackrel{\text{def}}{=} C([-\tau, 0], \mathbb{R}^{1+p})$, $\tau \geq 0$ denote the space of continuous functions from the interval $[-\tau, 0]$ into $\mathbb{R}^{1+p}$. Consider the following autonomous delay differential equation

$$\frac{d}{dt}y(t) = \mathcal{L}y_t + F(y_t), \quad t \geq 0, \tag{49}$$

where $y_t(\theta) = [x(t+\theta), \mu_1(t+\theta), \ldots, \mu_p(t+\theta)]^T \in X$, $-\tau \leq \theta \leq 0$, $\mathcal{L} : X \to \mathbb{R}^{1+p}$ is a bounded linear operator, and $F \in C^r(X, \mathbb{R}^{1+p})$, $r \geq 1$ is some smooth nonlinearity with $F(0) = 0$ and $DF(0) = 0$. Note that (49) should be viewed as a suspended system where the p parameters are included as dynamic variables with trivial dynamics. For our purposes, the dimension p of the parameter space for the suspended system will equal 1 or 2, depending on the bifurcation under study. The linearization of equation (49) about the trivial equilibrium is given by

$$\frac{d}{dt}y(t) = \mathcal{L}y_t, \quad t \geq 0. \tag{50}$$

Since $\mathcal{L}$ is a bounded linear operator from X into $\mathbb{R}^{1+p}$, it follows from Riesz's Theorem that $\mathcal{L}$ can be represented by a Riemann-Stieltjes integral

$$\mathcal{L}\phi = \int_{-\tau}^{0} [d\eta(\theta)]\, \phi(\theta), \quad \phi \in X, \tag{51}$$

where $\eta(\theta), -\tau \leq \theta \leq 0$, is a $(1+p) \times (1+p)$ matrix whose elements are of bounded variation. We may then rewrite equation (50) in the following form

$$\frac{d}{dt}y(t) = \int_{-\tau}^{0} [d\eta(\theta)]\, y(t+\theta), \quad t \geq 0. \tag{52}$$

Define $X' = C([0,\tau], \mathbb{R}^{(1+p)*})$, where $\mathbb{R}^{(1+p)*}$ is a space of row vectors. The transpose of equation (52) is (see formula (1.8), Chapter 7 of Hale and Lunel)

$$\frac{d}{dt}y(t) = -\int_{-\tau}^{0} y(t-\theta)[d\eta(\theta)], \quad t \leq 0, \quad y_0 = \psi \in X'. \tag{53}$$

For $\phi \in X$ and $\psi \in X'$, the following bilinear form is defined:

$$\langle \psi, \phi \rangle = \psi(0)\phi(0) - \int_{-\tau}^{0} \int_{0}^{\theta} \psi(\xi - \theta)\, [d\eta(\theta)]\, \phi(\xi)\, d\xi. \tag{54}$$

In the definition of the bilinear form as stated above, the integral over $d\eta(\theta)$ is performed last (with integration limits $-\tau$ to zero).

Since (49) has p components with trivial dynamics, then the characteristic equation corresponding to equation (50) always has p eigenvalues on the imaginary axis (at the origin). Thus, at a bifurcation, this characteristic equation has $m+p$ eigenvalues (counting multiplicity) on the imaginary axis and we will assume that all other eigenvalues have negative real parts. Then there exists an $(m+p)$-dimensional centre subspace $P \subset X$ for equation (52) which is invariant under the semi-flow for (50). We will denote a basis for P by the $(1+p) \times (m+p)$ matrix Φ; the columns of Φ are the basis vectors. There is a corresponding $(m+p)$-dimensional subspace P' of X' of solutions to the transposed equation (53). We will denote a basis for P' by the $(m+p) \times (1+p)$ matrix Ψ'. Hale and Lunel have shown [19] that the $(m+p) \times (m+p)$ matrix $\langle \Psi', \Phi \rangle$ is always nonsingular. We then define a new basis Ψ for P' by $\Psi = \langle \Psi', \Phi \rangle^{-1} \Psi'$ so that $\langle \Psi, \Phi \rangle = I$. The space X can be split as

$$X = P \oplus Q,$$

where Q is infinite-dimensional and invariant under the semi-flow for (50). It can then be shown using integral manifold techniques [19] that there exists a locally exponentially attracting $(m+p)$-dimensional centre manifold M_F for equation (49) given by

$$M_F = \{\phi \in X : \phi = \Phi z + h(z, F),\ z \text{ in a neighbourhood of zero in } \mathbb{R}^{m+p}\},$$

where $h(z, F) \in Q$ for each z and is a C^{r-1} function of z. The flow on this centre manifold is given by

$$y_t = \Phi z(t) + h(z(t), F),$$

and z satisfies the ordinary differential equation

$$\frac{d}{dt}z = Bz + \Psi(0)F(\Phi z + h(z, F)), \tag{55}$$

where the $(m+p) \times (m+p)$ matrix B satisfies the relation

$$\frac{d}{d\theta}\Phi = \Phi B. \tag{56}$$

That is, B is a matrix with eigenvalues with zero real parts and correspond to the solutions to the characteristic equation that lie on the imaginary axis (B is unique once Φ is specified). Therefore, the flow of the $(m+p)$-dimensional system (55) approximates well the long term behaviour of the flow of the full nonlinear infinite-dimensional system (49) near the origin. This is the framework in which we will study the bifurcations of the trivial equilibrium in (1).

Chapter 5

Pitchfork bifurcation

We have seen that the trivial equilibrium for (2) undergoes a pitchfork bifurcation when $\alpha = -1$ and $\tau \neq 1$. Thus, in this Chapter we treat α as a bifurcation parameter near -1, and we assume that τ is fixed and not equal to 1. Using the notation of the previous Chapter, we thus have $m = 1$ and $p = 1$. We may rewrite equation (2) in the following form

$$\begin{aligned} \frac{d}{dt}x(t) &= x(t) - x(t-\tau) + \mu x(t-\tau) + \gamma_1 x(t)^3 + \gamma_2 x(t)^2 x(t-\tau) + \\ &\quad \gamma_3 x(t) x(t-\tau)^2 + \gamma_4 x(t-\tau)^3 + O(|x|^5), \\ \frac{d}{dt}\mu(t) &= 0, \end{aligned} \tag{57}$$

where we have set $\alpha = \mu - 1$. Linearizing (57) at the trivial equilibrium, we get the following

$$\begin{aligned} \frac{d}{dt}x(t) &= x(t) - x(t-\tau), \\ \frac{d}{dt}\mu(t) &= 0. \end{aligned} \tag{58}$$

We may write the right hand side of (58) in integral form as follows:

$$\mathcal{L}\phi_t = \int_{-\tau}^{0} [d\eta(\theta)]\, \phi_t(\theta), \quad \phi_t \in X, \tag{59}$$

where

$$d\eta(\theta) = \begin{pmatrix} \delta(\theta) - \delta(\theta+\tau) & 0 \\ 0 & 0 \end{pmatrix} d\theta \tag{60}$$

and $\phi_t(\theta) = (x(t+\theta), \mu(t+\theta))^T$. Next, we note that the transposed system to equations (58) is

$$\frac{d}{dt}x(t) = -x(t) + x(t+\tau), \quad \frac{d}{dt}\mu(t) = 0. \tag{61}$$

A basis for the centre subspace of the linear system (58) is

$$\Phi = \begin{pmatrix} 1 & 0 \\ 0 & 1 \end{pmatrix},$$

and a basis for the transposed system (61) is

$$\Psi' = \Phi^T = \begin{pmatrix} 1 & 0 \\ 0 & 1 \end{pmatrix}.$$

The bilinear form (54) for this problem is given by (see Appendix A for the derivation of this bilinear form)

$$\langle \psi, \phi \rangle = \psi(0)\phi(0) - \int_{-\tau}^{0} \psi(\xi+\tau) \begin{pmatrix} 1 & 0 \\ 0 & 0 \end{pmatrix} \phi(\xi)\, d\xi. \tag{62}$$

We then compute

$$\langle \Psi', \Phi \rangle = \begin{pmatrix} 1-\tau & 0 \\ 0 & 1 \end{pmatrix}$$

and

$$\langle \Psi', \Phi \rangle^{-1} = \begin{pmatrix} \frac{1}{1-\tau} & 0 \\ 0 & 1 \end{pmatrix}.$$

We let

$$\Psi = \langle \Phi^T, \Phi \rangle^{-1} \Phi^T = \begin{pmatrix} \frac{1}{1-\tau} & 0 \\ 0 & 1 \end{pmatrix},$$

be a basis for the transposed system to equations (58). We note that the matrix $\langle \Psi, \Phi \rangle$ is the 2×2 identity matrix, as required. Also, the matrix

$$B = \begin{pmatrix} 0 & 0 \\ 0 & 0 \end{pmatrix},$$

satisfies relation (56). Write $z = [z_1, \mu]^T$ for the coordinates on the centre manifold. Finally, we note that the nonlinear terms in (57) can be written as

$$\begin{aligned} F([v_1, v_2]^T) &= [v_2(0)\, v_1(-\tau) + \gamma_1 v_1(0)^3 + \gamma_2 v_1(0)^2 v_1(-\tau) + \\ &\quad \gamma_3 v_1(0) v_1(-\tau)^2 + \gamma_4 v_1(-\tau)^3 + O(|v|^5), 0]^T. \end{aligned} \tag{63}$$

Retaining up to first order terms in μ, and up to third order terms overall, we get the following equations on the centre manifold

$$\frac{d}{dt} z_1 = \frac{1}{1-\tau}[\mu z_1 + (\gamma_1 + \gamma_2 + \gamma_3 + \gamma_4) z_1^3] \tag{64}$$

$$\frac{d}{dt} \mu = 0 \tag{65}$$

Note that the denominator $1 - \tau$ of (64) is non-zero if and only if $\tau \neq 1$. Thus, the above reduction breaks down (as expected) at this point which, as we will see, is in fact a Takens-Bogdanov point. Generically, the cubic coefficient $(\gamma_1 + \gamma_2 + \gamma_3 + \gamma_4)$ is non-zero, and thus (64) is a normal form for a pitchfork bifurcation. In terms of the original model parameters in (2), equation (64) becomes

$$\frac{d}{dt} z_1 = \frac{1}{1-\tau}[(\alpha + 1) z_1 + (\gamma_1 + \gamma_2 + \gamma_3 + \gamma_4) z_1^3]. \tag{66}$$

We have thus proved the following.

Theorem 2 *In equation (2), assume that* $\gamma_1 + \gamma_2 + \gamma_3 + \gamma_4 \neq 0$, *and* $\tau \neq 1$. *Then the local dynamics of (2) near the origin and for* α *near* -1 *reduces to the pitchfork bifurcation normal form (66), regardless of the* $O(|x(t)|^5)$ *term in (2).*

Chapter 6

Hopf bifurcation

We now suppose that (α_0, τ_0) is a point on the top boundary curve in Figure 1. In this case equation (5) has a pair of purely imaginary roots, and all other roots have negative real parts. We rewrite equation (2) as

$$\begin{aligned} \frac{d}{dt}x(t) &= x(t) + \alpha_0 x(t-\tau_0) + \mu x(t-\tau_0) + \gamma_1 x(t)^3 + \\ &\quad \gamma_2 x(t)^2 x(t-\tau_0) + \gamma_3 x(t) x(t-\tau_0)^2 + \gamma_4 x(t-\tau_0)^3 + O(|x|^5), \\ \frac{d}{dt}\mu(t) &= 0, \end{aligned} \tag{67}$$

where we have set $\alpha = \mu + \alpha_0$. The linearization of this equation at the trivial equilibrium is

$$\begin{aligned} \frac{d}{dt}x(t) &= x(t) + \alpha_0 x(t-\tau_0), \\ \frac{d}{dt}\mu(t) &= 0. \end{aligned} \tag{68}$$

We may write the right hand side of (68) in integral form as follows:

$$\mathcal{L}\phi_t = \int_{-\tau_0}^{0} [d\eta(\theta)]\, \phi_t(\theta), \quad \phi_t \in X, \tag{69}$$

where

$$d\eta(\theta) = \begin{pmatrix} \delta(\theta) + \alpha_0\, \delta(\theta + \tau_0) & 0 \\ 0 & 0 \end{pmatrix} d\theta \tag{70}$$

and $\phi_t(\theta) = (x(t+\theta), \mu(t+\theta))^T$. The transposed system to equations (68) is written as

$$\frac{d}{dt}x(t) = -x(t) - \alpha_0 x(t+\tau_0), \quad \frac{d}{dt}\mu(t) = 0. \tag{71}$$

A basis for the centre subspace of the linear system (68) is

$$\Phi = \begin{pmatrix} \sin(\omega_0\theta) & \cos(\omega_0\theta) & 0 \\ 0 & 0 & 1 \end{pmatrix},$$

and a basis for the transposed system (71) is

$$\Psi' = \Phi^T = \begin{pmatrix} \sin(\omega_0\theta) & 0 \\ \cos(\omega_0\theta) & 0 \\ 0 & 1 \end{pmatrix},$$

where $\omega_0 = \sqrt{\alpha_0^2 - 1}$ by (9). The bilinear form (54) reduces to (see Appendix A for derivation of bilinear form)

$$\langle \psi, \phi \rangle = \psi(0)\phi(0) + \alpha_0 \int_{-\tau_0}^{0} \psi(\xi + \tau_0) \begin{pmatrix} 1 & 0 \\ 0 & 0 \end{pmatrix} \phi(\xi)\, d\xi. \tag{72}$$

We then compute

$$\langle \Psi', \Phi \rangle = \begin{pmatrix} \frac{1-\tau_0}{2} & \frac{-\omega_0\tau_0}{2} & 0 \\ \frac{\omega_0\tau_0}{2} & \frac{1-\tau_0}{2} & 0 \\ 0 & 0 & 1 \end{pmatrix}$$

and

$$\langle \Psi', \Phi \rangle^{-1} = \frac{4}{(1-\tau_0)^2 + (\omega_0\tau_0)^2} \begin{pmatrix} \frac{1-\tau_0}{2} & \frac{\omega_0\tau_0}{2} & 0 \\ \frac{-\omega_0\tau_0}{2} & \frac{1-\tau_0}{2} & 0 \\ 0 & 0 & 1 \end{pmatrix},$$

where we have made use of (8). We let

$$\Psi = \langle \Phi^T, \Phi \rangle^{-1} \Phi^T = \kappa \begin{pmatrix} \frac{(1-\tau_0)\sin(\omega_0\theta) + \omega_0\tau_0\cos(\omega_0\theta)}{2} & 0 \\ \frac{-\omega_0\tau_0\sin(\omega_0\theta) + (1-\tau_0)\cos(\omega_0\theta)}{2} & 0 \\ 0 & \kappa^{-1} \end{pmatrix} \stackrel{\text{def}}{=} \begin{pmatrix} b_1(\theta) & 0 \\ b_2(\theta) & 0 \\ 0 & 1 \end{pmatrix},$$

be a basis for the transposed system to equations (68), where $\kappa = 4/((1-\tau_0)^2 + (\omega_0\tau_0)^2)$. It can easily be checked that the matrix

$$B = \begin{pmatrix} 0 & -\omega_0 & 0 \\ \omega_0 & 0 & 0 \\ 0 & 0 & 0 \end{pmatrix},$$

satisfies relation (56). Write $z = [z_1, z_2, \mu]^T$ for the coordinates on the centre manifold. The nonlinear terms in (67) are given by

$$\begin{aligned} F([v_1, v_2]^T) &= [v_2(0)v_1(-\tau_0) + \gamma_1 v_1(0)^3 + \gamma_2 v_1(0)^2 v_1(-\tau_0) + \\ &\quad \gamma_3 v_1(0)v_1(-\tau_0)^2 + \gamma_4 v_1(-\tau_0)^3 + O(|v|^5), 0]^T. \end{aligned} \tag{73}$$

Substituting the above results into equation (55) and truncating, we get the following ordinary differential equations on the centre manifold

$$\begin{aligned} \frac{d}{dt}z_1 &= -\omega_0 z_2 + b_1(0)[\mu(-\sin(\omega_0\tau_0)z_1 + \cos(\omega_0\tau_0)z_2) + \gamma_1 z_2^3 \\ &\quad +\gamma_2 z_2^2(-\sin(\omega_0\tau_0)z_1 + \cos(\omega_0\tau_0)z_2) \\ &\quad +\gamma_3 z_2(-\sin(\omega_0\tau_0)z_1 + \cos(\omega_0\tau_0)z_2)^2 \\ &\quad +\gamma_4(-\sin(\omega_0\tau_0)z_1 + \cos(\omega_0\tau_0)z_2)^3] \end{aligned} \tag{74}$$

$$\begin{aligned} \frac{d}{dt}z_2 &= \omega_0 z_1 + b_2(0)[\mu(-\sin(\omega_0\tau_0)z_1 + \cos(\omega_0\tau_0)z_2) + \gamma_1 z_2^3 \\ &\quad +\gamma_2 z_2^2(-\sin(\omega_0\tau_0)z_1 + \cos(\omega_0\tau_0)z_2) \\ &\quad +\gamma_3 z_2(-\sin(\omega_0\tau_0)z_1 + \cos(\omega_0\tau_0)z_2)^2 \\ &\quad +\gamma_4(-\sin(\omega_0\tau_0)z_1 + \cos(\omega_0\tau_0)z_2)^3] \end{aligned} \tag{75}$$

$$\frac{d}{dt}\mu = 0. \tag{76}$$

Now consider the linear part (in (z_1, z_2)) of equations (74) and (75),

$$\frac{d}{dt}z = B'z, \tag{77}$$

where

$$B' = \begin{pmatrix} -b_1(0)\mu\sin(\omega_0\tau_0) & -\omega_0 + b_1(0)\mu\cos(\omega_0\tau_0) \\ \omega_0 - b_2(0)\mu\sin(\omega_0\tau_0) & b_2(0)\mu\cos(\omega_0\tau_0) \end{pmatrix},$$

and where we have redefined z such that $z = [z_1, z_2]^T$. By a linear change of variables in z, the matrix B' can be brought into the following Jordan normal form

$$B'' = \begin{pmatrix} c_1 & -c_2 \\ c_2 & c_1 \end{pmatrix},$$

where, for example, to first order in μ

$$c_1 = \frac{1}{2}\mu(b_2(0)\cos(\omega_0\tau_0) - b_1(0)\sin(\omega_0\tau_0)). \tag{78}$$

After a further (nonlinear) change of variables the equations on the centre manifold can be brought into normal form and truncated at third order to give

$$\frac{d}{dt}z_1 = (c_1 + a(z_1^2 + z_2^2))z_1 - (c_2 + b(z_1^2 + z_2^2))z_2, \tag{79}$$

$$\frac{d}{dt}z_2 = (c_2 + b(z_1^2 + z_2^2))z_1 + (c_1 + a(z_1^2 + z_2^2))z_2, \tag{80}$$

where a and b are constants. In polar coordinates these equations simplify further and become

$$\frac{d}{dt}r = c_1 r + ar^3, \tag{81}$$

$$\frac{d}{dt}\theta = c_2 + br^2. \tag{82}$$

The first Liapunov coefficient a can be computed and is given by

$$a(\mu) = \frac{1}{2[(1-\tau_0)^2 + (\omega_0\tau_0)^2]}[\gamma_1(3/2 - 3\tau_0/2) + \gamma_2(\alpha_0\tau_0/2 + \tau_0/\alpha_0 - 3/(2\alpha_0)) + \gamma_3(1/2 - 3\tau_0/2 + 1/\alpha_0^2) + \gamma_4(3\alpha_0\tau_0/2 - 3/(2\alpha_0))] + O(\mu), \tag{83}$$

where the constants α_0, τ_0, and ω_0 are such that equations (8) are satisfied.

Equations (79)-(80) are a normal form for the standard Hopf bifurcation provided that the first Liapunov coefficient $a(0)$ and the eigenvalue crossing speed $\partial c_1/\partial\mu|_{\mu=0}$ are both finite and non-zero. We immediately see that this breaks down (as expected) at the point $(\alpha_0, \tau_0) = (-1, 1)$, which will be shown below to be a Takens-Bogdanov point. A straightforward computation reveals that for all $(\alpha_0, \tau_0) \neq (-1, 1)$ on the

Hopf curve, we have $\partial c_1/\partial \mu|_{\mu=0} > 0$, so the crossing condition is always satisfied. However, the coefficient $a(0)$ can be zero at isolated points on the Hopf curve away from the Takens-Bogdanov point. The exact places where this occurs will depend on the values of the coefficients $\gamma_i, 1 \leq i \leq 4$. At such points, (79)-(80) are no longer a normal form for the Hopf bifurcation (fifth order terms are required). We have thus proved the following.

Theorem 3 *In equation (2), assume that* $(\alpha, \tau) = (\alpha_0, \tau_0) \neq (-1, 1)$ *are such that (8) is satisfied for some* $\omega_0 \neq 0$. *Furthermore, assume that* γ_i, $1 \leq i \leq 4$ *are such that* $a(0) \neq 0$ *in (83). Then the local dynamics of (2) near the origin and for* α *near* α_0 *reduces to the Hopf bifurcation normal form (81)-(82), regardless of the* $O(|x(t)|^5)$ *term in (2).*

Chapter 7

Takens-Bogdanov bifurcation

In this Chapter, we will compute a centre manifold/normal form reduction of (2) near the point $(\alpha, \tau) = (-1, 1)$, and show that the trivial equilibrium undergoes a Takens-Bogdanov bifurcation at this point. Since this singularity has codimension 2, we perform the centre manifold suspension with both parameters. By rescaling time in units of the delay we may rewrite equation (2) in the following form

$$\begin{aligned}
\frac{d}{dt}x(t) &= x(t) - x(t-1) + \mu_2[x(t) - x(t-1)] + (1+\mu_2)[\mu_1 x(t-1) + \\
&\quad \gamma_1 x(t)^3 + \gamma_2 x(t)^2 x(t-1) + \gamma_3 x(t) x(t-1)^2 + \\
&\quad \gamma_4 x(t-1)^3 + O(|x|^5)] \qquad (84)\\
\frac{d}{dt}\mu_1(t) &= 0,\\
\frac{d}{dt}\mu_2(t) &= 0,
\end{aligned}$$

where we have set $\alpha = \mu_1 - 1$ and $\tau = \mu_2 + 1$. Linearizing (84) yields

$$\begin{aligned}
\frac{d}{dt}x(t) &= x(t) - x(t-1)\\
\frac{d}{dt}\mu_1(t) &= 0, \qquad (85)\\
\frac{d}{dt}\mu_2(t) &= 0.
\end{aligned}$$

We may write the right hand side of (85) in integral form as follows:

$$\mathcal{L}\phi_t = \int_{-1}^{0} [d\eta(\theta)]\, \phi_t(\theta), \quad \phi_t \in X, \tag{86}$$

where

$$d\eta(\theta) = \begin{pmatrix} \delta(\theta) - \delta(\theta+1) & 0 & 0 \\ 0 & 0 & 0 \\ 0 & 0 & 0 \end{pmatrix} d\theta \tag{87}$$

and $\phi_t(\theta) = (x(t+\theta), \mu_1(t+\theta), \mu_2(t+\theta))^T$. The transposed system to equations (85) is

$$\frac{d}{dt}x(t) = -x(t) + x(t+1), \quad \frac{d}{dt}\mu_1(t) = 0, \quad \frac{d}{dt}\mu_2(t) = 0. \tag{88}$$

A basis for the centre subspace of the linear system (85) is

$$\Phi = \begin{pmatrix} 1 & \theta & 0 & 0 \\ 0 & 0 & 1 & 0 \\ 0 & 0 & 0 & 1 \end{pmatrix},$$

and a basis for the transposed system (88) is

$$\Psi' = \Phi^T = \begin{pmatrix} 1 & 0 & 0 \\ \theta & 0 & 0 \\ 0 & 1 & 0 \\ 0 & 0 & 1 \end{pmatrix}.$$

The bilinear form (54) reduces to (see Appendix A for derivation of bilinear form)

$$\langle \psi, \phi \rangle = \psi(0)\phi(0) - \int_{-1}^{0} \psi(\xi+1) \begin{pmatrix} 1 & 0 & 0 \\ 0 & 0 & 0 \\ 0 & 0 & 0 \end{pmatrix} \phi(\xi)\, d\xi, \tag{89}$$

We then compute

$$\langle \Psi', \Phi \rangle = \begin{pmatrix} 0 & 1/2 & 0 & 0 \\ -1/2 & 1/6 & 0 & 0 \\ 0 & 0 & 1 & 0 \\ 0 & 0 & 0 & 1 \end{pmatrix}$$

and

$$\langle \Psi', \Phi \rangle^{-1} = \begin{pmatrix} 2/3 & -2 & 0 & 0 \\ 2 & 0 & 0 & 0 \\ 0 & 0 & 1 & 0 \\ 0 & 0 & 0 & 1 \end{pmatrix}.$$

Let

$$\Psi = \langle \Phi^T, \Phi \rangle^{-1} \Phi^T = \begin{pmatrix} 2/3 - 2\theta & 0 & 0 \\ 2 & 0 & 0 \\ 0 & 1 & 0 \\ 0 & 0 & 1 \end{pmatrix},$$

be a new basis for the transposed system to equations (85). It can easily be checked that the matrix

$$B = \begin{pmatrix} 0 & 1 & 0 & 0 \\ 0 & 0 & 0 & 0 \\ 0 & 0 & 0 & 0 \\ 0 & 0 & 0 & 0 \end{pmatrix},$$

satisfies relation (56). We write $z = [z_1, z_2, \mu_1, \mu_2]^T$ for the coordinates on the centre manifold. Finally, we note that the nonlinear terms in (84) are given by

$$\begin{aligned} F([v_1, v_2, v_3]^T) &= [v_3(0)\,(v_1(0) - v_1(-1)) + (1 + v_3(0))\,(v_2(0)\,v_1(-1) + \\ &\quad \gamma_1 v_1(0)^3 + \gamma_2 v_1(0)^2 v_1(-1) + \gamma_3 v_1(0) v_1(-1)^2 \\ &\quad + \gamma_4 v_1(-1)^3 + O(|v|^5)), 0, 0]^T. \end{aligned} \tag{90}$$

Retaining up to first order terms in μ_1 and μ_2, and up to third order terms overall, we get the following truncated equations on the centre manifold

$$\frac{d}{dt} z_1 = z_2 + \frac{2}{3}[\mu_2\, z_2 + \mu_1\,(z_1 - z_2) + a_1\, z_1^3 + a_2\, z_1^2\, z_2 + a_3\, z_1\, z_2^2 + a_4\, z_2^3] \tag{91}$$

$$\frac{d}{dt} z_2 = 2\,[\mu_2\, z_2 + \mu_1\,(z_1 - z_2) + a_1\, z_1^3 + a_2\, z_1^2\, z_2 + a_3\, z_1\, z_2^2 + a_4\, z_2^3] \tag{92}$$

$$\frac{d}{dt} \mu_1 = 0 \tag{93}$$

$$\frac{d}{dt}\mu_2 = 0, \tag{94}$$

where

$$a_1 = \gamma_1 + \gamma_2 + \gamma_3 + \gamma_4 \tag{95}$$

$$a_2 = -\gamma_2 - 2\gamma_3 - 3\gamma_4 \tag{96}$$

$$a_3 = \gamma_3 + 3\gamma_4 \tag{97}$$

$$a_4 = -\gamma_4. \tag{98}$$

Equations (91) to (94) can be simplified by the following near-identity nonlinear transformation of coordinates $z \to z + h_3(z)$ to normal form (see Chapter 3 for details), where

$$h_3(z) = \begin{pmatrix} ((1/3)\,a_3 + (2/9)\,a_2)\,z_1^3 + ((1/3)\,a_3 + a_4)\,z_1^2 z_2 + (2/3)\,a_4\,z_1 z_2^2 \\ (-2/3)\,a_1\,z_1^3 + a_3\,z_1^2 z_2 + 2\,a_4\,z_1 z_2^2 \\ 0 \\ 0 \end{pmatrix}.$$

This transformation gives, to third order, the following equations on the centre manifold

$$\begin{aligned} \frac{d}{dt}z_1 &= z_2 \\ \frac{d}{dt}z_2 &= 2[\mu_2 z_2 + \mu_1(z_1 - (2/3)\,z_2) + (a_1 + a_2)\,z_1^2 z_2 + a_1\,z_1^3]. \end{aligned} \tag{99}$$

In terms of the original parameters, equations (99) become

$$\begin{aligned} \frac{d}{dt}z_1 &= z_2, \\ \frac{d}{dt}z_2 &= (2\alpha + 2)z_1 + (-4\alpha/3 + 2\tau - 10/3)\,z_2 \\ &\quad +2(\gamma_1 - \gamma_3 - 2\gamma_4)z_1^2 z_2 + 2(\gamma_1 + \gamma_2 + \gamma_3 + \gamma_4)z_1^3. \end{aligned} \tag{100}$$

Thus, comparing (100) and (17), we can immediately read off the relations between the original DDE parameters α, τ, γ_i, $i = 1, \ldots, 4$ and the parameters β_1, β_2, a and b in the versal unfolding (17) of the Takens-Bogdanov singularity with reflectional symmetry.

Thus, we have shown the following.

Theorem 4 *In equation (2), assume that the following generic conditions are satisfied*

$$\gamma_1 + \gamma_2 + \gamma_3 + \gamma_4 \neq 0, \quad \text{and} \quad \gamma_1 - \gamma_3 - 2\gamma_4 \neq 0,$$

Then the local dynamics of (2) near the origin and for (α, τ) *near* $(-1, 1)$ *reduces to the Takens-Bogdanov bifurcation normal form (100) (with phase diagram of Figure 2), regardless of the* $O(|x(t)|^5)$ *term in (2).*

Chapter 8

Applications to ENSO

This Chapter is devoted to the study of specific examples of equation (2) along with comparisons with numerical simulations. The simulations were done using a fixed-step fourth-order Runge-Kutta method with linear interpolation for the required two midpoint evaluations of the delayed variable. A range of time steps was used to ensure the accuracy of our simulations. In all cases, constant initial functions were used. See Appendix B for the FORTRAN code used to do the numerical simulations in this Chapter.

8.1 Example 1

The first case we study is that of a simple standard bistable system with delayed linear feedback. As mentioned in the Introduction, such equations have received attention in the context of the ENSO phenomenon, where they serve as a simple heuristic model known as the Delayed Action Oscillator [28]. It is also being investigated in the context of neural networks with intrinsic bistable elements. It has the form

$$\frac{d}{dt}x(t) = x(t) + \alpha x(t-\tau) - x(t)^3, \tag{101}$$

where $\alpha, \tau \in \mathbb{R}$, with $\tau > 0$. In the context of ENSO, the dependent variable x represents the sea surface temperature (SST) anomaly. The first term on the right-hand side represents unstable ocean-atmosphere perturbations, while the third term

represents the nonlinear effects that limit its growth (e.g., advective processes in the ocean and moist processes in the atmosphere). A side effect of the unstable ocean-atmosphere perturbations is the generation of oceanic waves. The delayed feedback term represents the effect of these oceanic waves (i.e. westward propagating Rossby waves on the ocean thermocline that, after reflecting from the western boundary, become eastward propagating Kelvin waves that reenter the coupled ocean-atmosphere system after a time delay equal to their transit time). Note that this model (equation (101)) is a special case of equation (2) with $(\gamma_1, \gamma_2, \gamma_3, \gamma_4) = (-1, 0, 0, 0)$. It follows immediately from our analysis in Chapter 7 that (101) falls into Case 2 of the Takens-Bogdanov classification (See Figure 2b). Indeed, we obtain the following equations on the centre manifold

$$\begin{aligned} \frac{d}{dt}z_1 &= z_2, \\ \frac{d}{dt}z_2 &= (2\alpha+2)z_1 + (-4\alpha/3 + 2\tau - 10/3)z_2 - z_1^2 z_2 - z_1^3. \end{aligned} \tag{102}$$

In addition to the trivial fixed point ($x = 0$), equation (101) has nontrivial fixed points at $x = \pm\sqrt{1+\alpha}$. We may do a linear stability analysis around these nontrivial fixed points to obtain more information about this system. In fact, by symmetry, we need only do the analysis for one of the nontrivial fixed points. Following the procedure in Chapter 2, we first "centre" equation (101) around the fixed point $x = \sqrt{1+\alpha}$ and neglect any nonlinear terms to get

$$\frac{d}{dt}y(t) = (-2 - 3\alpha)y(t) + \alpha y(t-\tau). \tag{103}$$

Substitution of the ansatz $y(t) = e^{\lambda t}$ into (103), where λ is a complex parameter, gives the characteristic equation

$$\lambda = -2 - 3\alpha + \alpha e^{-\lambda\tau}. \tag{104}$$

Again using A.5 of [19] we find that all roots of (104) have negative real parts if and only if

$$\begin{aligned} &2\tau + 3\alpha\tau > -1 \\ &2\tau + 2\alpha\tau > 0 \\ &\alpha\tau > -\zeta\sin\zeta + (2\tau + 3\alpha\tau)\cos\zeta, \end{aligned} \tag{105}$$

where ζ is the root of $\zeta = -(2\tau + 3\alpha\tau)\tan\zeta$, $0 < \zeta < \pi$, if $2\tau + 3\alpha\tau \neq 0$ and $\zeta = \pi/2$ if $2\tau + 3\alpha\tau = 0$. We now obtain Figure 6. The solid line for $\alpha < -1$

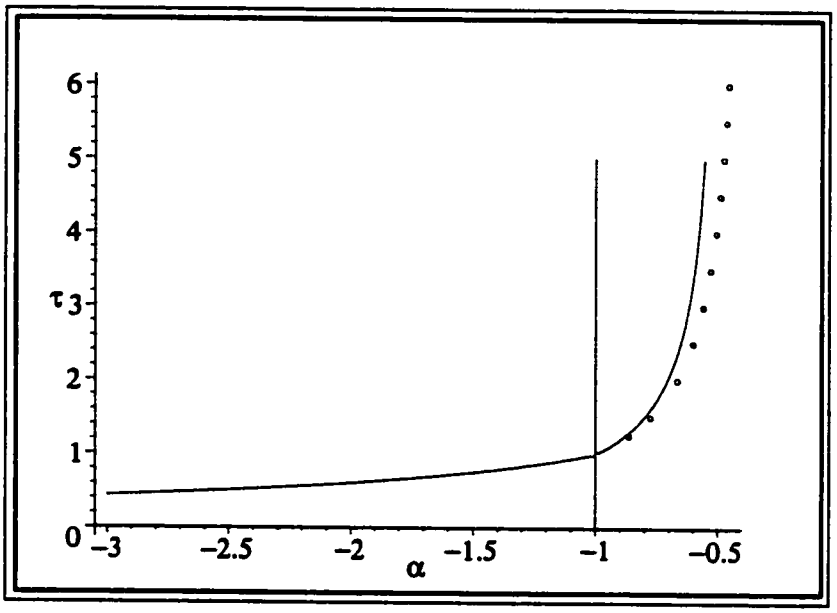

Figure 6: Bifurcation diagram for the "Delayed Oscillator" equation (101). This figure should be compared to Figure 2b. The solid line for $\alpha < -1$ is the Hopf bifurcation line for the trivial fixed point. The solid line for $\alpha > -1$ is the Hopf bifurcation line for the nontrivial fixed points (i.e. $\pm\sqrt{1+\alpha}$). The line $\alpha = -1$ is the pitchfork bifurcation line. The dots are numerical simulations of equation (101) approximating the bifurcation curve labelled S in Figure 2b. Note that line C from Figure 2b has not been plotted. Indeed, this line is difficult to determine in DDE (101) because the distinguishing features in regions 4 and 5 are unstable and only appear as transients.

is the Hopf bifurcation line for the trivial fixed point which we already met. The solid line for $\alpha > -1$ is the Hopf bifurcation line for the nontrivial fixed points (i.e. $\pm\sqrt{1+\alpha}$) obtained via equations (105). This is the same line as in Figure 2 of [28]. The line $\alpha = -1$ is the pitchfork bifurcation line. The dots are numerical simulations of equation (101) approximating the bifurcation curve labelled S in Figure 2b. This curve is a nonlinear effect (a saddle node of periodic orbits), and we cannot obtain an expression for this curve via a linear stability analysis near the fixed points. Note also that line C in Figure 2b has not been plotted. Indeed, regions 4 and 5

would be difficult to distinguish with numerical simulations of DDE (101) because the structures which would distinguish them (limit cycles around the nontrivial fixed points in Region 4 and a large amplitude limit cycle in Region 5) are unstable. These unstable effects could only be seen as transients. However, close to the Takens-Bogdanov point, for parameter values on line C in Figure 2b, we simulated the DDE (101); the results are shown in figure 7.

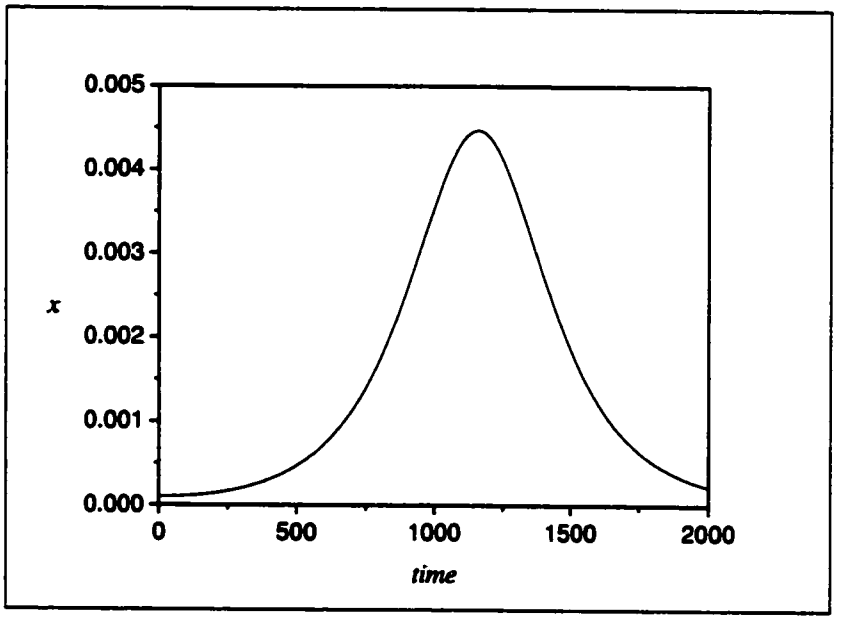

Figure 7: Numerical solution to equation (101) for parameters "on" line C of figure 2(b) ($\alpha = -0.99999, \tau = 1.000014667$) very close to the Takens-Bogdanov point. For parameters on line C equation (101) has an (unstable) double saddle connection at the trivial equilibrium. Solutions on this line have infinite period. In this figure we can detect the presence of this saddle connection by the large period of the solution. The vertical scale is x and the horizontal scale is time t.

It is interesting to note that in [28] Suarez and Schopf (from now they will be referred to as SS) claim "This simple system [referring to equation (101)] has multiple stationary states which can all become unstable. When this happens, solutions are self-sustained oscillations whose period is at least twice as long as the assumed delay". This statement may lead one to believe that it is only when the nontrivial fixed

points become unstable that this large amplitude oscillation results, i.e. that the large amplitude oscillation will only appear by crossing the solid line (in the direction of increasing τ) to the right of $\alpha = -1$ in Figure 6, when in fact our analysis has shown that the large amplitude oscillation will appear before (for smaller values of the delay) the nontrivial fixed points become unstable, and there will be a region of tristability (two stable fixed points and a stable limit cycle). Indeed, numerical simulations support our claim (see Figure 8). In other words, the large amplitude oscillation will appear by crossing the dotted line in Figure 6 to the right of the line $\alpha = -1$ as the delay is increased from zero.

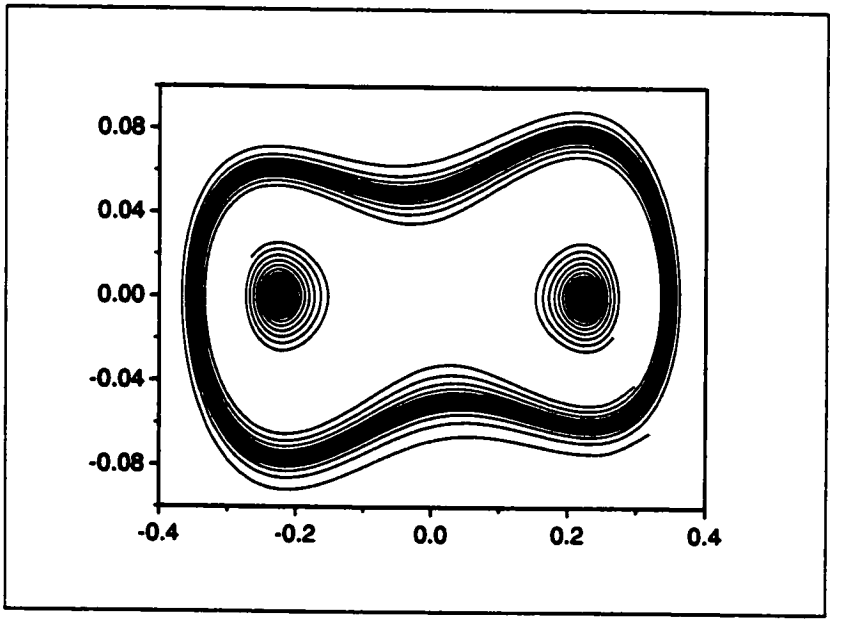

Figure 8: Multistability: Numerical simulation of (101) with $(\alpha, \tau) = (-19/20, 647/600)$. These parameter values fall in Region 4 of Figure 2b, where the DDE exhibits tristability. The vertical axis is $\dot{x}$ and the horizontal axis is x.

In that same paper the authors study the period of the oscillations as a function of the delay. Indeed, they obtain Figure 9. SS wish to demonstrate that the period of the large amplitude limit cycle is everywhere greater than two times the delay and their figure seems to support this claim. However upon closer inspection, the solid line in their figure is obtained by a linear stability analysis of the nontrivial

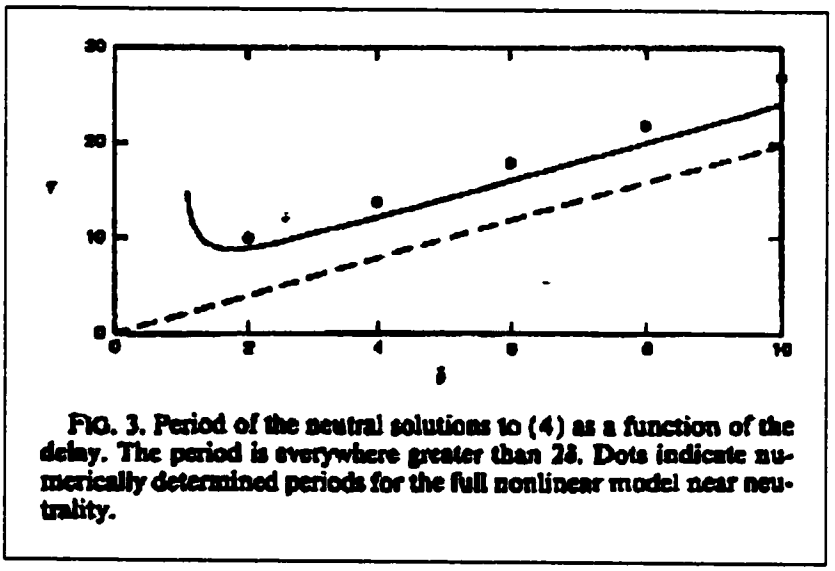

Figure 9: Figure 3 from [28]. The figure shows how the period of the large amplitude (amplitude denoted by τ in this figure) oscillation found in equation (101) changes as a function of the delay (denoted by δ in this figure). This figure was reprinted with permission from the American Meteorological Society.

fixed points, which while giving information about the period of the unstable limit cycles generated around the nontrivial fixed points, does not provide any information about the large amplitude oscillations! So their figure does not provide any evidence for their claim, other than the fact that the dots obtained by numerical simulations seem to agree with it. So how does one obtain information about the period of the large amplitude oscillation? This is not a completely trivial problem. We know from our work in Chapter 3 that for parameter values on Line S in Figure 2b (close to the Takens-Bogdanov point), the large amplitude limit cycle found in (101) has an "energy" value of $h_s \approx 0.089$ (see Figure 5). Solving for v in equation (38) (and ignoring the negative root) we get

$$v = \frac{1}{2}\sqrt{8h_s + 4u^2 - 2u^4}. \tag{106}$$

Substituting this result into the first equation in (37) we get the following separable

differential equation

$$\frac{d}{dt}u = \frac{1}{2}\sqrt{8h_s + 4u^2 - 2u^4} \tag{107}$$

Therefore

$$T_{h_s} = 2\int_{-\sqrt{1+\sqrt{1+4h_s}}}^{\sqrt{1+\sqrt{1+4h_s}}} \frac{u}{\frac{1}{2}\sqrt{8h_s + 4u^2 - 2u^4}}\,du, \tag{108}$$

where T_{h_s} is the period of the large amplitude periodic orbit that appears on line S in (b) of the Takens-Bogdanov classification. This however is not the period of the large amplitude oscillation that appears in our original DDE because we have scaled time by a factor of $\sqrt{2\alpha+2}$ (see (35)). The period we are after is then given by $T_{h_s}/\sqrt{2\alpha+2}$. Finally, we wish to obtain an expression for the period as a function of the delay τ, not α. We can obtain this expression by using equation (48). We get following expression

$$T = 2\frac{\sqrt{2+3c}}{\sqrt{6(\tau-1)}}\int_{-\sqrt{1+\sqrt{1+4h_s}}}^{\sqrt{1+\sqrt{1+4h_s}}} \frac{u}{\frac{1}{2}\sqrt{8h_s + 4u^2 - 2u^4}}\,du, \tag{109}$$

where T is the period of the large amplitude oscillation, $c \approx 0.752$, and $h_s \approx 0.089$. This integral can easily be evaluated numerically with programs like MAPLE (see figure 10).

In Figure 10, the solid curve is the curve given by equation (109). The straight line originating from the origin is the line $T = 2\tau$, and the dots are numerical simulations of equation (101) for parameter values on the line of saddle node bifurcations of periodic orbits, i.e. for parameter values of the dotted line in Figure 6. This Figure should be compared with Figure 9 taken from [28]. Note that equation (109) is only accurate for τ very close to, but larger than 1. In fact, we see that this equation starts to diverge from numerical results for $\tau > 1.3$. So it seems that the conjecture of SS, that the period of the large amplitude oscillation is everywhere greater then 2τ is true, as least for say $1 \leq \tau \leq 10$. But what happens as τ approaches infinity? SS say "for large values of [the delay], the solutions approach a square wave, with a period of twice the delay". Our numerical simulations agree with their statement (see Figure 11). We have tried to prove that this is indeed the case, but had little success. So we leave it as an open conjecture for now.

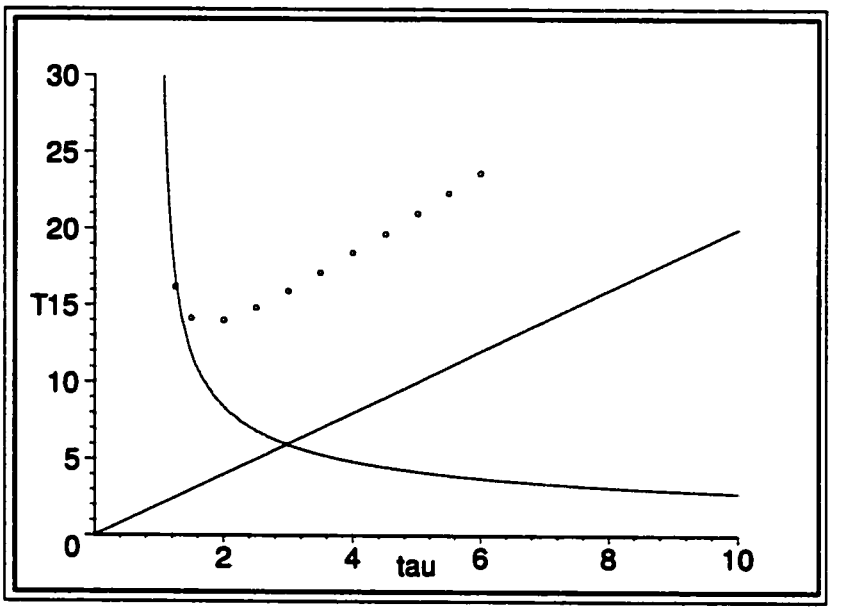

Figure 10: This figure shows how the period of the large amplitude (T) oscillation found in equation (101) changes as a function of the delay (τ). The solid curve is given by equation (109) and the diagonal line is the line $T = 2\tau$. The points are numerical simulations of equation (101) for parameter values on the line of saddle node bifurcations of periodic orbits. This figure should be compared to the previous one taken from [28].

Conjecture 1 *The period of the large amplitude oscillation which appears by a saddle node bifurcation of periodic orbits in equation (101) as the delay is increased (and $\alpha > -1$) is everywhere greater than twice the delay. Further, solutions approach a square wave of period exactly twice the delay as the delay approaches infinity.*

Numerical simulations strongly suggest that this conjecture is true. If we assume that it is true, what more can be said about equation (101)? Consider the following heuristic argument. Rescaling time in units of delay equation (101) becomes

$$\frac{d}{dt}\frac{x(t)}{\tau} = x(t) + \alpha x(t-1) - x(t)^3. \tag{110}$$

Letting $\tau \to \infty$, the equation simplifies to

$$x(t)^3 - x(t) = \alpha x(t-1), \tag{111}$$

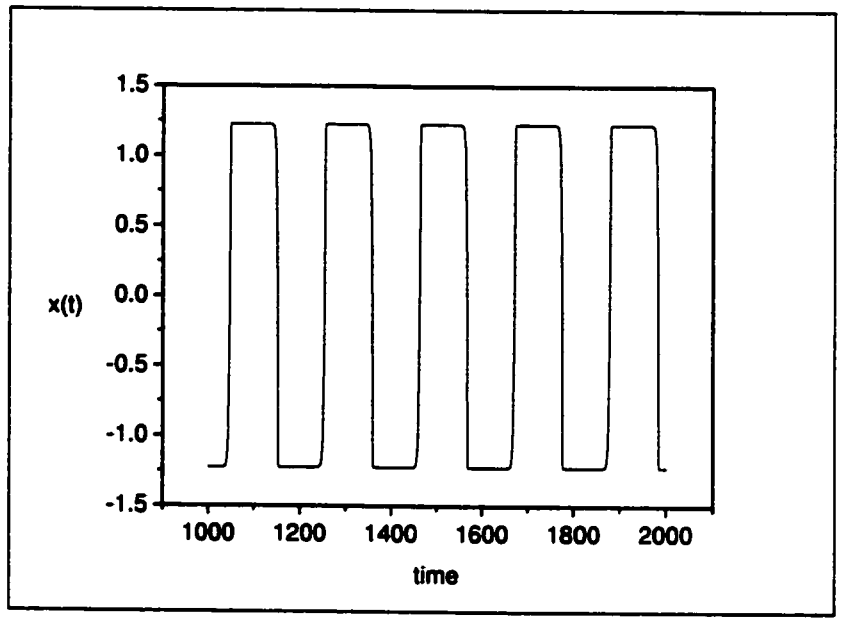

Figure 11: Solutions to equation (101) approach square waves for $-\infty < \alpha < 0.5$ when the delay gets large. This figure shows a numerical solution to equation (101) with $\alpha = -0.5$ and $\tau = 100$. Note that the period is only slightly greater than twice the delay, and the amplitude is $\sqrt{1-\alpha} \approx 1.225$.

from which we obtain the following "map"

$$x_{n+1}^3 - x_{n+1} = \alpha x_n. \tag{112}$$

Now this "map" is not well-defined. Divide through by x_{n+1} to obtain

$$x_{n+1}^2 - 1 = \alpha \frac{x_n}{x_{n+1}}. \tag{113}$$

Suppose now that conjecture 1 is true. Then, by the symmetry of equation (101), we see that $x_n/x_{n+1} = -1$, so that we may solve equation (113) to get

$$x_{n+1} = (-1)^n \sqrt{1-\alpha}. \tag{114}$$

This map correctly predicts the behaviour of equation (101) for $\alpha > -1$, in the limit of large delay. Further, it predicts that the amplitude of the oscillation will be $\sqrt{1-\alpha}$ (again see figure 11).

This concludes our analysis of equation (101). It should also be mentioned that Battisti and Hirst in [1] argue for use of the parameter range $\alpha < -1$. We will refer to parameter values with $\alpha < -1$ as region R_2, and with $\alpha > -1$ as region R_1. This follows the notation of Battisti and Hirst. Operating equation (101) in either regime, R_1 or R_2, will yield similar effects. Both will produce a large amplitude oscillation as the delay is increased. However, the oscillation produced in R_2 is via a Hopf bifurcation. And we can obtain limit cycles of arbitrarily small amplitude. In contrast, the limit cycle produced in R_1 appears with finite amplitude, and the amplitude does not vary much as the delay is increased. Further, in Region R_1 there exists a region of tristability–a stable limit cycle and stable El Niño and La Niña states. With a further increase in the delay the El Niño and La Niña states remain, but are unstable. In Region R_1 no such El Niño or La Niña states exists. We expect these differences will become more pronounced when noise and periodic forcing are added to the system. As for which regime more realistically models ENSO, we will have to wait for further investigations to determine this.

8.2 Example 2

In Battisti and Hirst [1], the authors analyze a simple coupled ocean-atmosphere model. They argue that the essential physics in this model can be described by a linear delayed oscillator (the Suarez and Schopf model without the cubic nonlinearity)

$$\frac{d}{dt}x(t) = x(t) + \alpha x(t-\tau). \tag{115}$$

They proceed in identifying the leading order correction (see [1]) to the linear oscillator (115) and obtain the following DDE

$$\frac{d}{dt}x(t) = x(t) + \alpha\, x(t-\tau) - e[x(t) - r x(t-\tau)]^3. \tag{116}$$

Finally, they consider equation (116) when the nonlinear damping depends only on the instantaneous temperature $x(t)$ (i.e. set $r = 0$ in (116)) and obtain

$$\frac{d}{dt}x(t) = x(t) + \alpha\, x(t-\tau) - e x(t)^3. \tag{117}$$

In all cases, x represents the SST anomaly, and e and r are positive real parameters. As in [1] we will study each of these equations in turn.

Equation (115) does not fall into our classification scheme because the non-degeneracy conditions (see Chapter 7) are not satisfied. However, the linear stability analysis of Chapter 2 still holds. Battisti and Hirst use parameter range R_2 when studying this equation. For this parameter range we see from Figure 1 that equation (115) undergoes a "Hopf" bifurcation, in the sense that a pair of complex eigenvalues cross the imaginary axis with non-zero speed as the delay is increased, and all other eigenvalues have negative real parts. However, there is no nonlinearity to limit its growth and we obtain unbounded oscillations. Of course, Battisti and Hirst would agree that this is a nonphysical result, but argue that it is this bifurcation (a linear effect) that accounts for the ENSO oscillation, and that any nonlinear term primarily acts to bound the amplitude of the oscillations. They state that "the fundamental frequency of ENSO events is determined by linear processes". Note that this is in direct opposition to SS who argue that the ENSO oscillation appears for parameters in R_1, where we have showed that the oscillations appears via a saddle node bifurcation of periodic orbits (a nonlinear effect) so that the fundamental frequency of ENSO is determined by nonlinear processes.

As mentioned above, equation (116) contains the leading order correction to the linear model equation (115). Note that this model is a special case of equation (2) with $(\gamma_1, \gamma_2, \gamma_3, \gamma_4) = (-e, 3er, -3er^2, er^3)$. Provided $r \neq 1$ and $e \neq 0$, our results from Chapter 7 show that near the point $(\alpha, \tau) = (-1, 1)$ in parameter space equation (116) is well approximated near the trivial equilibrium by the centre manifold equations

$$\begin{aligned} \frac{d}{dt}z_1 &= z_2, \\ \frac{d}{dt}z_2 &= (2\alpha+2)z_1 + (-4\alpha/3 + 2\tau - 10/3)z_2 + \\ &\quad (-e + 3er^2 - 2er^3)z_1^2 z_2 + (-e + 3er - 3er^2 + er^3)z_1^3. \end{aligned} \tag{118}$$

It can easily be shown that regardless of the value of the parameter e in equation (116), the coefficient of the $z_1^2 z_2$ term in equations (118) will be negative for all values of $r \neq 1$, and that the coefficient of the z_1^3 term in equations (118) will be negative if

$r < 1$ and will be positive if $r > 1$. To summarize, if $r > 1$ then the dynamics near the Takens-Bogdanov point are described in Figure 2a, and if $r < 1$ then the dynamics near the Takens-Bogdanov point are described in Figure 2b. In [1] the authors use a value of r that is less than 1. Their model therefore falls into Case 2 of the Takens-Bogdanov classification (see Figure 2b). Qualitatively this more complicated model behaves similarly to the SS model, equation (101), at least for parameters values near the Takens-Bogdanov point.

Finally we consider equation (117) which is the same equation postulated by SS (see equation (101)). This model has already been studied in depth in the previous section. We again note, however, that although this equation is the same as the SS model, Battisti and Hirst operate this model with parameter values in the range R_1. It is important to note that it is not simply a disagreement about parameter values that BH operate their model in R_2 and not R_1. The BH model highlights a very different balance in the fundamental processes than the SS model. It is not currently known which is the better model of the two.

As an aside, we want to mention that equation (116) has recently appeared in [24] with parameters $(\alpha, e, r) = (-1, 1, 1)$. In that paper the author studies a model for a single-mode semiconductor laser with weak optical feedback, in which he shows resonant behavior caused by the interplay of noise and delayed feedback. He then goes on to argue that this resonant behaviour is not particular to the model equations used by showing the same effects in equation (116) with the parameters mentioned above. But with these parameters, equation (116) is highly degenerate and does not fall into the Takens-Bogdanov classification scheme (the nondegeneracy conditions in Theorem 4 are not satisfied) . This means that its dynamics are not described by Figure 2 and fifth-order terms must be considered in the analysis. So perhaps the effect is a peculiarity of the high degeneracy of equation (116) and the model equation? Based on the work done in [30] however, it seems that this resonant effect is in fact quite general. But it is interesting nevertheless to note another context in which this class of delay equations is being studied.

Chapter 9

Conclusions and future work

We have performed a bifurcation analysis of a class of first order nonlinear delay-differential equations with reflectional symmetry. Our results reveal the presence of a Takens-Bogdanov bifurcation point which acts as an organizing centre around the origin. Our results are also original in that they also provide the unfolding of this bifurcation in terms of the parameters of the original DDE. This was made possible due to our centre manifold analysis of the suspended DDE, i.e. of the DDE augmented with the (trivial) parameter dynamics.

Future work will involve looking into the origin of chaotic behaviour that we have found numerically. Specifically, consider the following DDE which is again a special case of equation (2) with $(\gamma_1, \gamma_2, \gamma_3, \gamma_4) = (0, -2, 1, 0)$

$$\frac{d}{dt}x(t) = x(t) + \alpha\, x(t-\tau) - 2\, x(t)^2\, x(t-\tau) + x(t)\, x(t-\tau)^2. \qquad (119)$$

Since $\gamma_1 - \gamma_3 - 2\gamma_4 = -1$ and $\gamma_1 + \gamma_2 + \gamma_3 + \gamma_4 = -1$, we fall into Case 2 of the Takens-Bogdanov classification (See Figure 2b). It can easily be verified with equation (83) that near the Takens-Bogdanov point the Hopf bifurcation is supercritical (that is, the coefficient a in equation (81) is negative). Far from this point, however, the criticality may change. In fact, the Hopf coefficient a is positive if $\alpha < -1.65$ approximately. Near the point where the Hopf coefficient a is null the DDE exhibits what seems to be chaotic behaviour (to be investigated later). For example, let $(\alpha, \tau) = (-1.65, 0.705)$. Figure 12 is a numerical simulation of the DDE with these parameter values.

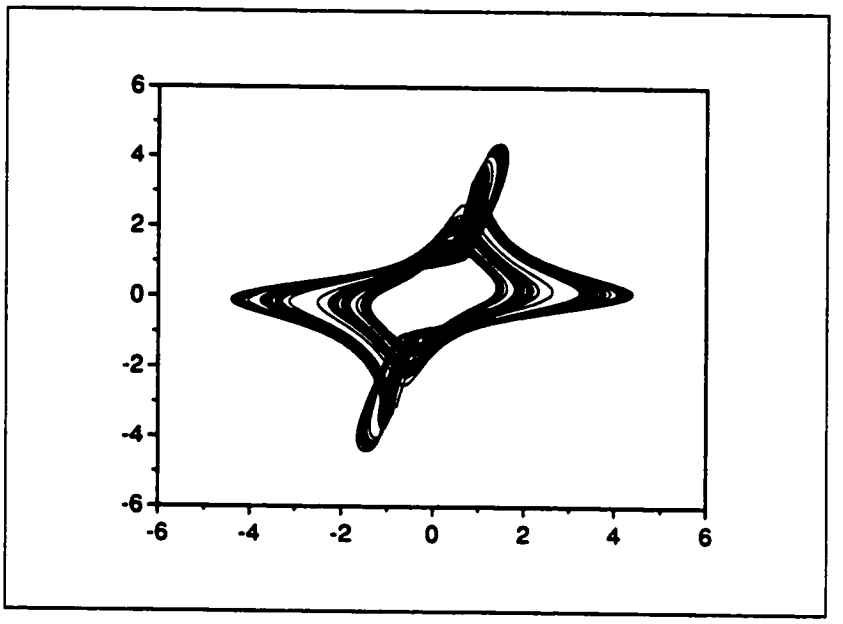

Figure 12: Chaotic solution to the DDE? Numerical simulation of (119) with $(\alpha, \tau) = (-1.65, 0.705)$. The vertical axis is x_τ and the horizontal axis is x.

Future work will address increasingly more realistic models for ENSO. For example, we can modify the "Delayed Action Oscillator" as follows

$$\frac{d}{dt}x(t) = x(t) + \alpha\, x(t-\tau) - x(t)^3 + A\cos(2\pi f t) + \sqrt{2D}\xi(t), \qquad (120)$$

where the cosine term of amplitude A represents the interaction of annual seasonal forcing, and $\xi(t)$ is Gaussian white noise with $\langle\xi\rangle = 0$ and $Var(\xi) = 1$ which represents random (say day-to-day) environmental fluctuations. The above equation has been studied by [30], but in the context of noise-induced dynamics. They find that the linear response to the external periodic force has maxima at the frequencies corresponding to the inverse delay time and its harmonics (and subharmonics). It is expected that many of the results obtained in this context would be of interest to the ENSO community who may be able to provide a physical understanding of these resonant effects.

More recent models for ENSO (see e.g. [27]) have added a delay to the unstable $x(t)$ term in equation (101) to represent an eastward propagating Kelvin wave which

reflects off the South American coast and reenters the system after a delay time strictly less than the delay time for the westward propagating Rossby wave. This leads to the study of a DDE with linear part

$$\frac{d}{dt}x(t) = x(t-\tau_1) + \alpha x(t-\tau_2), \tag{121}$$

where $\alpha \in \mathbb{R}$, with $\alpha < 0$, and $\tau_2 > \tau_1 > 0$. The difficulty in understanding equation (121) will reside in the linear stability analysis. This equation retains the reflectional symmetry. Thus, $x = 0$ is a fixed point. Substitution of the ansatz $x(t) = e^{\lambda t}$ into (121), where λ is a complex parameter, gives the characteristic equation

$$\lambda = e^{-\lambda\tau_1} + \alpha e^{-\lambda\tau_2}. \tag{122}$$

Setting $\lambda = i\omega$ in (122), and separating real and imaginary parts, we obtain the following equations

$$0 = \cos(\omega\tau_1) + \alpha\cos(\omega\tau_2), \tag{123}$$

$$\omega = -\sin(\omega\tau_1) - \alpha\sin(\omega\tau_2). \tag{124}$$

Solving these equations for α and τ_2, we get

$$\alpha = \pm\sqrt{\cos(\omega\tau_1)^2 + (\omega + \sin(\omega\tau_1)))^2}, \quad \tau_2 = \frac{\arctan\left(\frac{\omega+\sin(\omega\tau_1)}{\cos(\omega\tau_1)}\right) + k\pi}{\omega}, \tag{125}$$

where k is an integer. For a given value of τ_1, these equations can be used to plot parametrically (with parameter ω) the lines of purely imaginary eigenvalues in (α, τ_2)-space. One small technicality should be mentioned when plotting with these equations: For a given value of ω (and τ_1 and k), the sign of α must be chosen so as to satisfy equations (123) and (124). It remains to determine which of these curves define the region of stability for the equilibrium solution $x(t) = 0$. We know that when $\tau_1 = 0$, the characteristic equation (122) reduces to (5), the characteristic equation we studied in Chapter 2 with region of stability given in Figure 1. So by a continuity argument, the stability region for (122) should be very similar to Figure 1 when τ_1 is close to zero. Indeed, we can use this fact to show that the stability regions for $\tau_1 = 1, 2, 3, 4, 5$ are given by the hashed regions in Figures 13,14,15,16,17, respectively. It can also be checked that the Takens-Bogdanov bifurcation point occurs

at $(\alpha, \tau_1, \tau_2) = (-1, \tau_1, 1 + \tau_1)$ (simply check that the linearly independent functions $x(t) = 1$ and $x(t) = t$ are solution to equation (121) for these parameter values). It is interesting to see how the region of stability changes as the value of τ_1 increases, and to note the intersections of bifurcation curves which occur on the boundary of the stability region. For example, in Figure 17, near the point $(\alpha, \tau_2) = (-1.29, 0.62)$ we have the intersection of two Hopf bifurcation curves which leads to very interesting dynamics (see Figure 18). Also note in Figure 17 that the point $(\alpha, \tau_2) = (-1, 4)$ corresponds to the intersection of the Hopf bifurcation curves and the pitchfork bifurcation curve. Finally, in that same Figure we see that the Takens-Bogdanov point has become even more degenerate with the Hopf bifurcation curve looping back on itself and crossing the point where it originated. The point is that we can now apply the same analysis that was done in this thesis for the one-delay equation to these points. This further analysis may be of interest to the Atmospheric Science community.

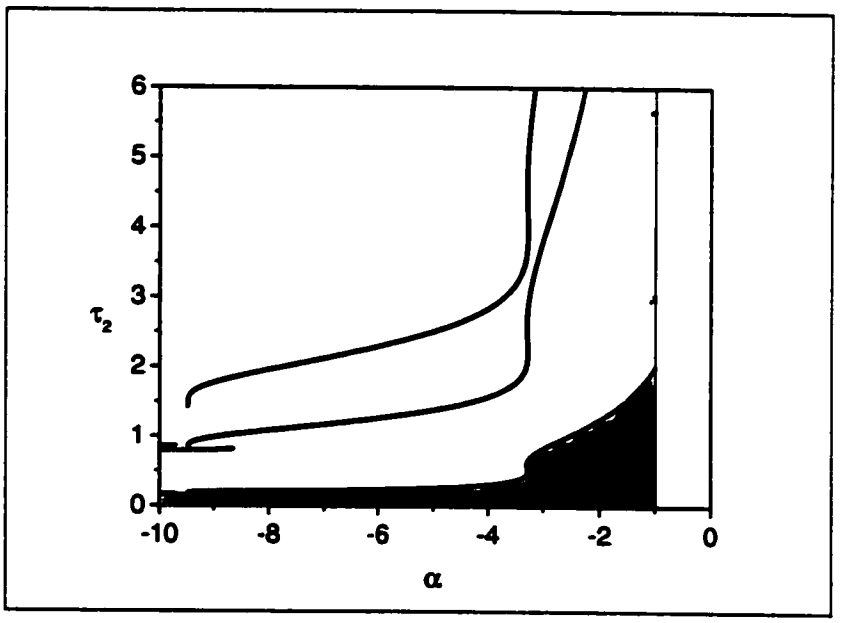

Figure 13: Stability region for equation (122) with $\tau_1 = 1$. For parameters on the other curves, the characteristic equation has purely imaginary roots, but also at least one eigenvalue with positive real part.

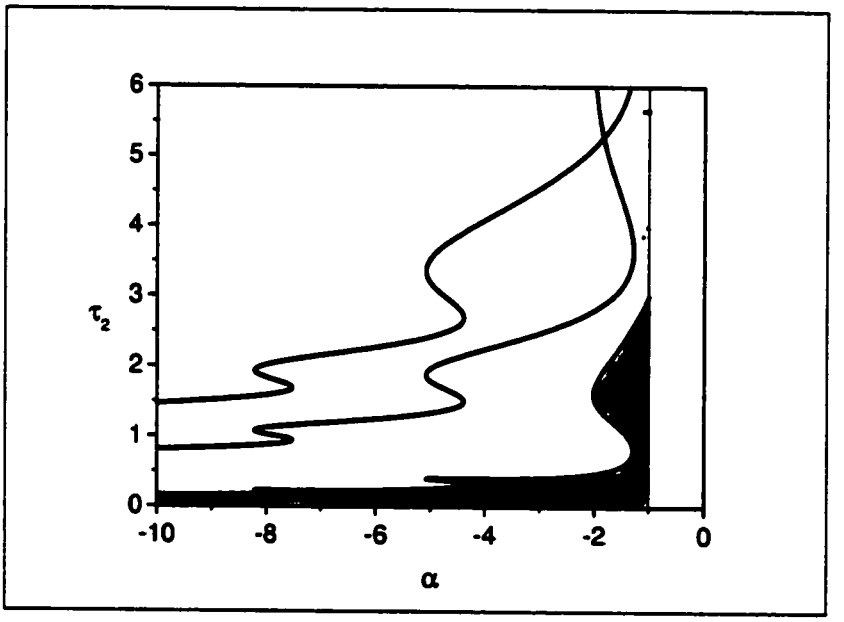

Figure 14: Stability region for equation (122) with $\tau_1 = 2$. For parameters on the other curves, the characteristic equation has purely imaginary roots, but also at least one eigenvalue with positive real part.

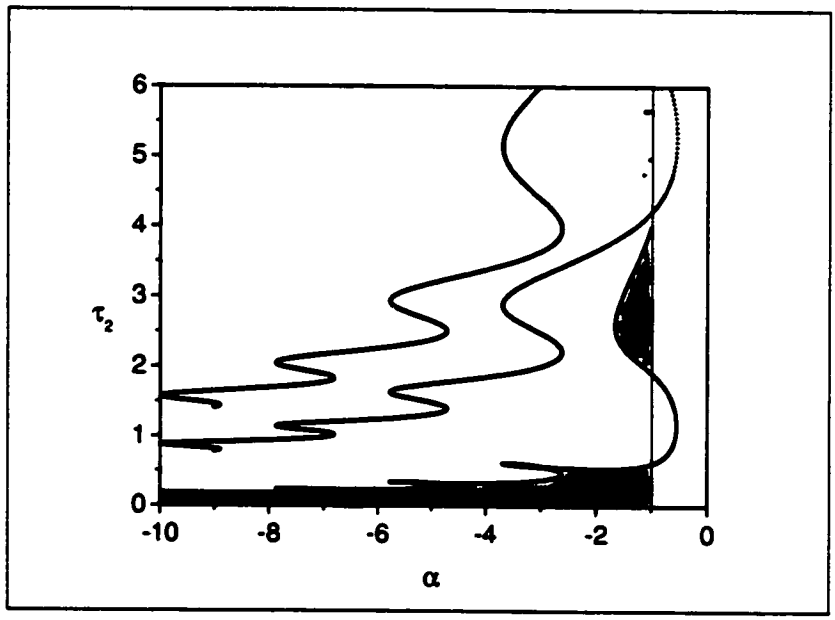

Figure 15: Stability region for equation (122) with $\tau_1 = 3$. For parameters on the other curves, the characteristic equation has purely imaginary roots, but also at least one eigenvalue with positive real part.

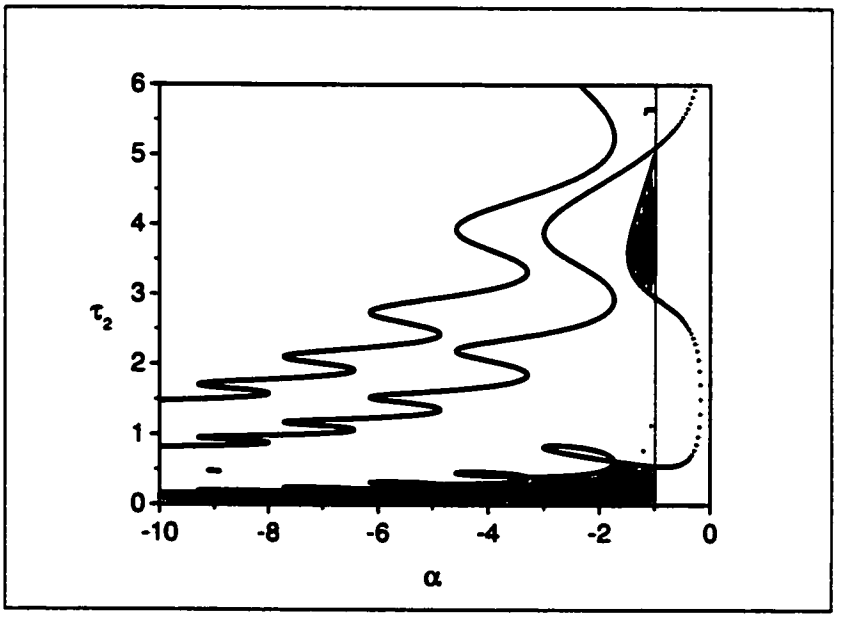

Figure 16: Stability region for equation (122) with $\tau_1 = 4$. For parameters on the other curves, the characteristic equation has purely imaginary roots, but also at least one eigenvalue with positive real part.

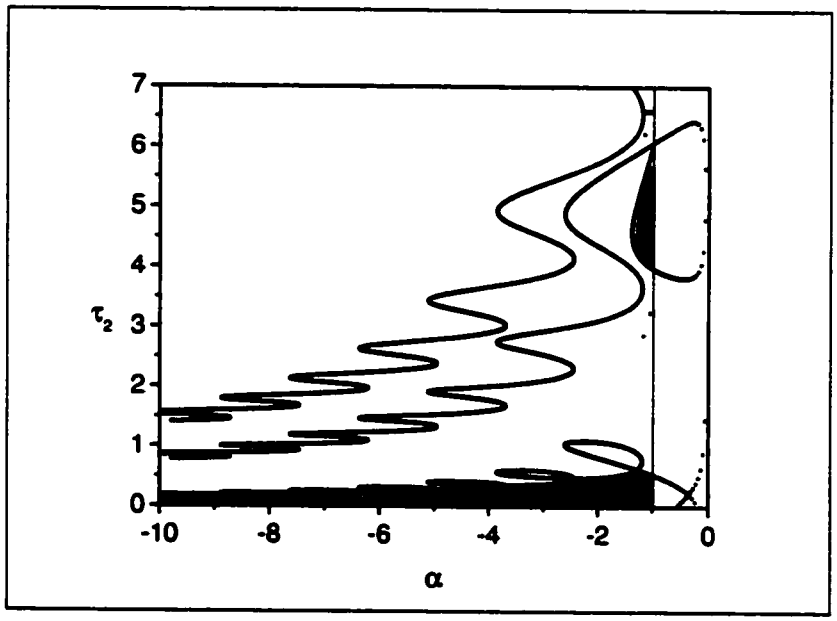

Figure 17: Stability region for equation (122) with $\tau_1 = 5$. For parameters on the other curves, the characteristic equation has purely imaginary roots, but also at least one eigenvalue with positive real part.

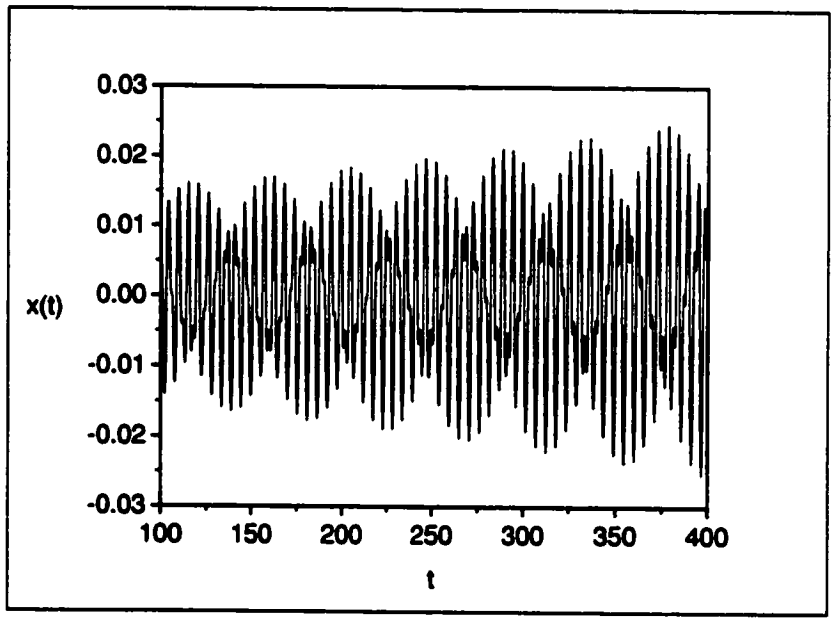

Figure 18: Double Hopf point. This figure is a numerical simulation of equation (121) near the point $\tau_1 = 5$, $\tau_2 = 0.62$, $\alpha = -1.29$ (see Figure 17). Note the effect of the two frequencies. The FORTRAN code in Appendix C was used to generate this figure.

Appendix A

Bilinear form

In chapter 4 we defined the following bilinear form

$$\langle \psi, \phi \rangle = \psi(0)\phi(0) - \int_{-\tau}^{0} \int_{0}^{\theta} \psi(\xi - \theta)\,[d\eta(\theta)]\,\phi(\xi)\,d\xi. \tag{126}$$

With this definition we will show how equations (62), (72) and (89) used in Chapters 5, 6 and 7, respectively, were found. We begin by changing the order of integration to obtain

$$\langle \psi, \phi \rangle = \psi(0)\phi(0) - \int_{-\tau}^{0} \int_{\xi}^{-\tau} \psi(\xi - \theta)\,[d\eta(\theta)]\,\phi(\xi)\,d\xi. \tag{127}$$

Reversing the limits of integration in the second integral, we get

$$\langle \psi, \dot{\phi} \rangle = \psi(0)\phi(0) + \int_{-\tau}^{0} \int_{-\tau}^{\xi} \psi(\xi - \theta)\,[d\eta(\theta)]\,\phi(\xi)\,d\xi. \tag{128}$$

For our problem we have

$$d\eta(\theta) = \left(\begin{array}{c|c} \alpha\,\delta(\theta+\tau) + \delta(\theta) & 0 \\ \hline 0 & N_0 \end{array}\right) d\theta, \tag{129}$$

where N_0 is the $p \times p$ zero matrix. Plugging this result back into (128), we obtain the following

$$\begin{aligned} \langle \psi, \phi \rangle = \psi(0)\phi(0) &+ \int_{-\tau}^{0} \int_{-\tau}^{\xi} \psi(\xi - \theta) \left(\begin{array}{c|c} \alpha\,\delta(\theta+\tau) & 0 \\ \hline 0 & N_0 \end{array}\right) d\theta\,\phi(\xi)\,d\xi \\ &+ \int_{-\tau}^{0} \int_{-\tau}^{\xi} \psi(\xi - \theta) \left(\begin{array}{c|c} \delta(\theta) & 0 \\ \hline 0 & N_0 \end{array}\right) d\theta\,\phi(\xi)\,d\xi. \end{aligned} \tag{130}$$

So we must consider the following two double integrals

$$\int_{-\tau}^{0}\int_{-\tau}^{\xi} \alpha\,\psi(\xi-\theta)\,\delta(\theta+\tau)d\theta\,\phi(\xi)\,d\xi, \tag{131}$$

and

$$\int_{-\tau}^{0}\int_{-\tau}^{\xi} \psi(\xi-\theta)\,\delta(\theta)d\theta\,\phi(\xi)\,d\xi. \tag{132}$$

In the first case, the only time the integrand is nonzero in the triangular region defined by the limits of integration (see Figure 19) is when $\theta = -\tau$ and $-\tau \leq \xi \leq 0$. So the first integral reduces to

$$\int_{-\tau}^{0} \alpha\,\psi(\xi+\tau)\phi(\xi)\,d\xi. \tag{133}$$

For the second integral, the only time the integrand is nonzero in the triangular region defined by the limits of integration (see Figure 19) is when $\theta = 0$ and $\xi = 0$, which is just one point. So the second integral is zero. Plugging these results back into equation (130), we obtain the following simplified bilinear form

$$\langle\psi,\phi\rangle = \psi(0)\phi(0) + \int_{-\tau}^{0} \psi(\xi+\tau)\left(\begin{array}{c|c} \alpha & 0 \\ \hline 0 & N_0 \end{array}\right)\phi(\xi)\,d\xi. \tag{134}$$

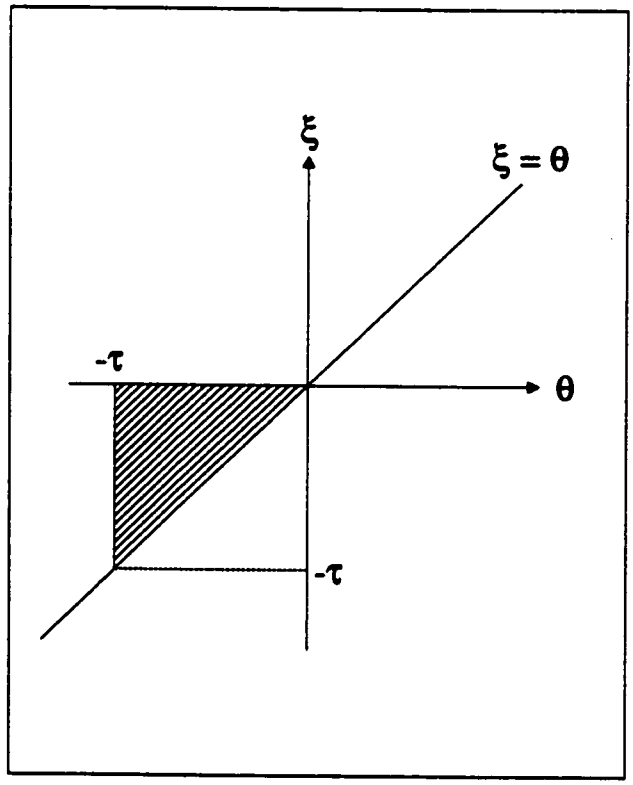

Figure 19: Region of integration.

Appendix B

Fortran code 1

This code numerically integrates a delay differential equation of the form

$$\frac{d}{dt}x(t) = x(t) + \alpha\, x(t-\tau) - x(t)^3$$

using a fourth-order Runge-Kutta integration method with linear interpolation for the required two midpoint evaluations of the delayed variable. Below is a commented printout of the FORTRAN code. Note that comments begin with the symbol "!".

```
!REAL VARIABLES
!xdel(1000000): a vector that records the values of x for one entire delay interval
!x: the value of x at one time
!dxdt: the RHS of DDE at one time
!xh: value of x after one iteration of rk4
!delt: step size of the delay interval
!tau: delay parameter
!xtau: x(t-tau)
!xtinit: initial condition
!realt: real time
!alph: parameter in DDE
```

```
!INTEGER VARIABLES
!deldiv: number of step sizes (delt) in one delay interval
!ntau: delay number counter
!ntaumax: maximum number of delays to run simulation
!k: a loop counter


! MAIN PROGRAM

program shn1
implicit none

! variable declarations

real*8 xdel(1000000),realt,alph
real*8 x,dxdt,xh,delt,tau,xtau,xtinit
integer deldiv,k,ntau,ntaumax

! global variables

common/eqparam/alph,xdel,delt,tau
common/deloop/k

! open and rewind the output file

open(6,file='mydata1.dat')
rewind 6

! set parameter values for simulation

alph=-1.5
```

```
tau=1.2
xtinit=1.0d-2
delt=1.0d0/1.0d3
ntaumax=100

! divide delay interval into 1/delt points

deldiv=ifix(sngl(1/delt))

! record initial condition in xdel

do 30 k=1,deldiv+1
xdel(k)=xtinit
30 continue

! start looping through delay intervals

do 100 ntau=1,ntaumax

! set x to value at far right of delay interval

x=xdel(deldiv+1)

! start looping through one delay interval

do 101 k=1,deldiv+1

! calculate the real time

realt=(ntau-1+(k-1)*delt)*tau
```

```
! set xtau to xdel(k)

xtau=xdel(k)

! output to file

write(6,001) realt,x,xtau
001 format(' ',6f15.10)

! call subroutine derivs to calculate the RHS of DDE

call derivs(realt,x,dxdt,xtau)

! call subroutine rk4 to calculate next value of x, output as xh

call rk4(x,dxdt,realt,xh)

! set xdel(k) to x

xdel(k)=x

! set x to xh calculated by rk4

x=xh

! end loop on k

101 continue

! end loop on ntau
```

```
100 continue

! close output file

close(6)

! end main program

stop
end

! subroutine to calculate the RHS of DDE

subroutine derivs(realt,x,dxdt,xtau)
implicit none
real*8 alph,xtau,x,dxdt,xdel(1000000),delt,tau,realt
common/eqparam/alph,xdel,delt,tau
dxdt=x+alph*xtau-x**3
return
end

! fourth-order Runge-Kutta integration subroutine, slightly
! modified to handle DDEs.

subroutine rk4(x,dxdt,realt,xh)
implicit none
real*8 x,dxdt,xh,xdel(1000000),realt,delt,tau
real*8 xt,dxt,dxm,hh,h6,th,tprime,xtau,alph
integer k
common/eqparam/alph,xdel,delt,tau
common/deloop/k
```

```
! the time step equals delt*tau
! F1,F2,F3,F4 represent the four calls to derivs needed in RK4

hh=delt*tau/2.0d0
h6=hh/3.0d0
th=realt+hh
xt=x+hh*dxdt !dxdt=F1!

! at this point we take xtau to be the average of
! xdel(k) and xdel(k+1). This is what is meant by "Linear
! interpolation for the required two midpoint evaluations (for F2 and F3) of
! the delayed variable".

xtau=(xdel(k)+xdel(k+1))/2.0d0 !=x(t+hh-tau)!
call derivs(th,xt,dxt,xtau) !F2=dxt!
xt=x+hh*dxt
call derivs(th,xt,dxm,xtau) !F3=dxm!
xt=x+delt*tau*dxm
dxm=dxt+dxm !F2+F3!

! for the last step take xtau=xdel(k+1) !=x(t+2*hh-tau)!

xtau=xdel(k+1)
tprime=realt+delt*tau
call derivs(tprime,xt,dxt,xtau) !F4=dxt!
xh=x+h6*(dxdt+dxt+2.0d0*dxm) !=x+hh/3*(F1+2*F2+2*F3+F4)!
return
end
```

Appendix C

Fortran code 2

This code numerically integrates a delay differential equation of the form

$$\frac{d}{dt}x(t) = x(t-\tau_1) + \alpha\, x(t-\tau_2)$$

with $\tau_1 \leq \tau_2$, using a simple Euler integration method. It was used to generate Figure 18. Again note that the symbol "!" begins a comment.

```
!REAL VARIABLES
!xdel(1000000): a vector that records the values of x for one
!large delay interval
!x: the value of x at one time
!dxdt: the RHS of DDE at one time
!xh: value of x after one iteration of euler
!delt: step size of the delay interval tau2
!tau1: the small delay parameter
!tau2: the large delay parameter
!xtau1: x(t-tau1)
!xtau2: x(t-tau2)
!xtinit: initial condition
!realt: real time
!alph: parameter in DDE
```

```
!INTEGER VARIABLES
!deldiv: number of step sizes (delt) in one large delay interval
!tau2
!ntau: large delay number counter
!ntaumax: maximum number of large delays to run simulation
!k: a loop counter
!d1: deldiv minus the number of delts in small delay interval tau1


! MAIN PROGRAM

program shn1
implicit none

! variable declarations

real*8 xdel(1000000),realt,alph
real*8 x,dxdt,xh,delt,tau1,tau2,xtau1,xtau2,xtinit
integer deldiv,k,ntau,ntaumax,d1

! global variables

common/eqparam/alph,xdel,delt,tau2
common/deloop/k

! open and rewind the output file

open(6,file='mydata1.dat')
rewind 6
```

```
! set parameter values for simulation

alph=-9.0d-1
tau1=1.0d-1
tau2=1.5d0
xtinit=1.0d-2
delt=1.0d0/1.0d4
ntaumax=40

! divide large delay interval into 1/delt points

deldiv=ifix(sngl(1/delt))

! record initial condition in xdel

do 30 k=1,deldiv+1
xdel(k)=xtinit
30 continue

! start looping through large delay intervals

do 100 ntau=1,ntaumax

! set x to value at far right of large delay interval

x=xdel(deldiv+1)

! start looping through one large delay interval

do 101 k=1,deldiv+1
```

```
! calculate the real time

realt=(ntau-1+(k-1)*delt)*tau2

! set xtau2 to xdel(k)

xtau2=xdel(k)

! calculate d1

d1=ifix(sngl((deldiv+1)*(1.0d0-tau1/tau2)))

! calculate xtau1

if (k.le.(deldiv+1)-d1) then
xtau1=xdel(k+d1)
else
xtau1=xdel(k-(deldiv+1)+d1)
endif

! output to file

write(6,001) realt,x,xtau1,xtau2
001 format(' ',4f15.10)

! call subroutine derivs to calculate the RHS of DDE

call derivs(realt,x,dxdt,xtau1,xtau2)

! call subroutine euler to calculate next value of x, output as xh
```

```
call euler(x,dxdt,realt,xh)

! set xdel(k) to x

xdel(k)=x

! set x to xh calculated by euler

x=xh

! end loop on k

101 continue

! end loop on ntau

100 continue

! close output file

close(6)

! end main program

stop
end

! subroutine to calculate the RHS of DDE

subroutine derivs(realt,x,dxdt,xtau1,xtau2)
implicit none
```

```
real*8 alph,xtau1,xtau2,x,dxdt,xdel(1000000),delt,tau2,realt
common/eqparam/alph,xdel,delt,tau2
dxdt=xtau1+alph*xtau2
return
end

! a simple euler integration subroutine

subroutine euler(x,dxdt,realt,xh)
implicit none
real*8 alph,x,dxdt,xh,xdel(1000000),realt,delt,tau2,hh
common/eqparam/alph,xdel,delt,tau2

! the time step equals delt*tau

hh=delt*tau2
xh=x+hh*dxdt
return
end
```

Bibliography

[1] D.S. Battisti and A.C. Hirst, Interannual Variability in a Tropical Atmosphere-Ocean Model: Influence of the Basic State, Ocean Geometry and Nonlinearity, *J. Atmos. Sci.* **46**, (1989) 1687-1712.

[2] J. Bélair, Stability in a model of a delayed neural network, *J. Dynam. Diff. Eq.* **5**, (1993) 607-623.

[3] J. Bélair and S.A. Campbell, Stability and bifurcations of equilibria in a multiple delayed differential equation, *SIAM J. Appl. Math.* **54**, (1994) 1402-1424.

[4] N.J. Berman and L. Maler, Neural architecture of the electrosensory lateral line lobe: Adaptations for coincidence detection, a sensory searchlight and frequency-dependent adaptive filtering, *J. Exper. Biol.* **202**, (1999) 1243-1253.

[5] P. C. Bressloff and C. V. Wood, Spontaneous oscillations in a nonlinear delayed-feedback shunting model of the pupil light reflex, *Phys. Rev. E* **58**, (1998) 3597-3606.

[6] P.C. Bressloff and S. Coombes, Symmetry and phase-locking in a ring of pulse-coupled oscillators with distributed delays, *Physica D* **126**, (1999) 99-122.

[7] A.R. Bulsara, E. Jacobs, T. Zhou, F. Moss and L. Kiss, Stochastic resonance in a single neuron model: theory and analog simulation, *J. Theor. Biol.* **154**, (1991) 531-555.

[8] S.A. Campbell, Stability and bifurcation of a simple neural network with multiple time delays, *Fields Institute Communic.* **21**, (1999) 65-79.

[9] J. Cao, Periodic oscillation and exponential stability of delayed Cellular Neural Networks (CNN's), *Phys. Lett. A* **270**, (2000) 157-163.

[10] J. Carr, *Applications of Centre Manifold Theory*, Springer-Verlag, New York (1981).

[11] Chinarov V. and Menzinger M. Computational dynamics of gradient bistable networks, *BioSystems* **55**, (2000) 137-142

[12] S.-N. Chow and J.K. Hale, *Methods of Bifurcation Theory*, Springer-Verlag, New York (1982).

[13] T. Faria and L.T. Magalhães, Normal Forms for Retarded Functional Differential Equations with Parameters and Applications to Hopf Bifurcation, *Journal of Differential Equations* **122**, (1995) 181-200.

[14] J.A. Freund, A.B. Neiman and L. Schimansky-Geier, Analytic description of noise-induced phase synchronization, *Europhys. Lett.* **50**, (2000) 8-14.

[15] F. Giannakopoulos and A. Zapp, Local and global Hopf bifurcation in a scalar delay differential equation, *Journal of Mathematical Analysis and Applications* **237**, (1999), no. 2, 425-450.

[16] K. Gopalsamy and I. Leung, Delay induced periodicity in a neural netlet of excitation and inhibition, *Physica D* **89**, (1996) 395-426.

[17] J. Guckenheimer and P. Holmes, *Nonlinear Oscillations, Dynamical Systems, and Bifurcations of Vector Fields*, Springer-Verlag, New York (1983).

[18] J.K. Hale, Flows on centre manifolds for scalar functional differential equations, *Proceedings of the Royal Society of Edinburgh* **101A**, (1985) 193-201.

[19] J.K Hale and S.V. Lunel, *Introduction to Functional Differential Equations*, Springer-Verlag, New York (1993).

[20] M. Kim *et al.*, Controlling chemical turbulence by global delayed feedback: Pattern formation in catalytic CO oxidation on Pt(110), *Science* **292**, (2001) 1357-1360.

[21] J.F. Lindner, B.K. Meadows and W.L. Ditto, Array enhanced stochastic resonance and spatiotemporal synchronization, *Phys. Rev. Lett.* **75**, (1995) 3-6.

[22] A. Longtin, A. Bulsara, D. Pierson, and F. Moss, Bistability and the dynamics of periodically forced sensory neurons, *Biol. Cybern.* **70**, (1994) 569-578.

[23] C.M. Marcus and R.M. Westerwelt, Stability of analog neural networks with delay, *Phys. Rev. A* **39**, (1989) 347-359.

[24] C. Masoller Noise-Induced Resonance in Delayed Feedback Systems, *Phys. Rev. Lett.* **88**(3), 034102 (2002).

[25] T. Ohira and Y. Sato, Resonance with noise and delay, *Phys. Rev. Lett.* **82**, (1999) 2811-2815.

[26] B.F. Redmond, V.G. LeBlanc, and A. Longtin, Bifurcation analysis of a class of first-order nonlinear delay-differential equations with reflectional symmetry, *Physica D*, **166**, (2002) 131-146.

[27] L. Stone and P.I. Saparin, Noise Induced Effects and Stochastic Resonance in an El Niño Model, *Applied Nonlinear Dynamics and Stochastic Systems Near the Millennium, J.B. Kadtke and A. Bulsara, eds., Amer. Inst. Physics Conf. Proc.*, **411**, (1997) 341-346.

[28] M.J. Suarez and P.L. Schopf, A Delayed Action Oscillator for ENSO, *J. Atmos. Sci.* **45**, (1988) 3283-3287.

[29] F. Takens, Forced Oscillations and Bifurcations, *Comm. Math. Inst. Rijkuniversiteit Utrecht* **3**, (1974b) 1-59.

[30] L.S. Tsimring and A. Pikovsky, Noise-Induced Dynamics in Bistable Systems with Delay, *Phys. Rev. Lett.* **87**(25), 250602 (2001).

[31] P. van den Driessche, J. Wu and X. Zou, Stabilization role of inhibitory self-connections in a delayed neural network, *Physica D* **150**, (2001) 84-90.

[32] J. Wei and S. Ruan, Stability and bifurcation in a neural network model with two delays, *Physica D* **130**, (1999) 255-272.

[33] J. Wu, Symmetric functional differential equations and neural networks with memory, *Trans. Am. Math. Soc.* **350**, (1999) 4799-4838.